

REPORT DOCUMENTATION PAGE

*Form Approved
OMB No. 0704-0188*

The public reporting burden for this collection of information is estimated to average 1 hour per response, including the time for reviewing instructions, searching existing data sources, gathering and maintaining the data needed, and completing and reviewing the collection of information. Send comments regarding this burden estimate or any other aspect of this collection of information, including suggestions for reducing the burden, to Department of Defense, Washington Headquarters Services, Directorate for Information Operations and Reports (0704-0188), 1215 Jefferson Davis Highway, Suite 1204, Arlington, VA 22202-4302. Respondents should be aware that notwithstanding any other provision of law, no person shall be subject to any penalty for failing to comply with a collection of information if it does not display a currently valid OMB control number.
PLEASE DO NOT RETURN YOUR FORM TO THE ABOVE ADDRESS.

1. REPORT DATE (DD-MM-YYYY) 30/06/2011			2. REPORT TYPE Final		3. DATES COVERED (From - To) 05/16/2007 - 05/30/2011	
4. TITLE AND SUBTITLE Mid-Frequency Sonar Interactions with Beaked Whales					5a. CONTRACT NUMBER	
					5b. GRANT NUMBER N00014-07-1-0992	
					5c. PROGRAM ELEMENT NUMBER	
6. AUTHOR(S) Kenneth G. Foote and Gonzalo R. Feijoo					5d. PROJECT NUMBER 13099200	
					5e. TASK NUMBER	
					5f. WORK UNIT NUMBER	
7. PERFORMING ORGANIZATION NAME(S) AND ADDRESS(ES) Applied Ocean Physics and Engineering Department Woods Hole Oceanographic Institution 98 Water Street Woods Hole, MA 02543-1053					8. PERFORMING ORGANIZATION REPORT NUMBER	
9. SPONSORING/MONITORING AGENCY NAME(S) AND ADDRESS(ES) Dr. James Eckman NOPP - Ocean Optics & Biology Program - Code 322 Office of Naval Research One Liberty Ctr. - Rm. 1073 875 N. Randolph Street Arlington, VA 22203-4590					10. SPONSOR/MONITOR'S ACRONYM(S) ONR	
					11. SPONSOR/MONITOR'S REPORT NUMBER(S)	
12. DISTRIBUTION/AVAILABILITY STATEMENT Approved for public release; distribution is unlimited						
13. SUPPLEMENTARY NOTES						
14. ABSTRACT See attached						
15. SUBJECT TERMS						
16. SECURITY CLASSIFICATION OF:			17. LIMITATION OF ABSTRACT	18. NUMBER OF PAGES	19a. NAME OF RESPONSIBLE PERSON	
a. REPORT	b. ABSTRACT	c. THIS PAGE			Kenneth G. Foote	
unclassified	unclassified	unclassified	unlimited		19b. TELEPHONE NUMBER (Include area code) 508-289-2445	

Mid-Frequency Sonar Interactions with Beaked Whales: Final Report

PI Kenneth G. Foote

Woods Hole Oceanographic Institution, 98 Water Street, Woods Hole, MA 02543
Phone: (508) 289-2445 FAX: (508) 457-2194 E-mail: kfoote@whoi.edu

Award Number: N000140710992

EXECUTIVE SUMMARY

Naval exercises involving use of military sonars operating in the mid-frequency (MF) band, 1-10 kHz, have been implicated in the strandings of marine mammals, especially beaked whales. Understanding the cause or causes of the greater sensitivity of beaked whales to MF sonar has stimulated much speculation and thought. The suspicion that there is a deep connection to anatomy instigated the project summarized here, namely "Mid-frequency sonar interactions with beaked whales." The ambition of this was to develop a tool that would enable researchers to predict sonar-induced acoustic fields inside beaked whales as well as inside other marine mammals. The tool, called the Virtual Beaked Whale, was to be an interactive online modeling and visualization system. Formidable resources were contributed to development of this system both by ONR and by the Woods Hole Oceanographic Institution, but it was not completed. However, the scope and components of such a system were outlined in detail, and some of these components were also developed. This included specification of a finite-element method (FEM) to solve the full-diffraction wave equation for acoustic interactions with a complicated, heterogeneous body; modeling the three-dimensional anatomy of exemplary marine mammal specimens; and assigning physical properties to the diverse, constituent tissues. Beaked whales are large: a mature Cuvier's beaked whale (*Ziphius cavirostris*) can be 8.5 m in length. This presents two difficulties. Firstly, detailed anatomical data cannot be obtained on a whole specimen by computed tomography (CT) scanning. Thus, a synthetic model of a beaked whale was developed based on CT scans of (i) the head of a freshly dead Cuvier's beaked whale, and (ii) the body of a harbour porpoise (*Phocoena phocoena*). Secondly, given MF wavelengths of order 0.15-1.5 m, the total number of equations to be solved is of order several tens of millions at the upper end of this band. This is a daunting number. Consequently, particular attention was paid to validation of the FEM model. For empirical validation, an experiment was performed at the Naval Surface Warfare Center, Carderock Division, in which an instrumented common dolphin (*Delphinus delphis*) cadaver was ensonified and internal fields measured in a number of tissues. In the course of this work the discovery was made that tourmaline sensors, which are ordinarily used to measure acoustic pressures at explosive shock levels, can also be used to measure weak, sub-shock pressures. For theoretical validation, provision was made for benchmarking through comparison with analytic solutions for internal acoustic and particle displacement fields due to ensonification of lossy fluid and solid elastic spheres by plane harmonic waves. Ultimately, the validated model was to serve as the heart of the Virtual Beaked Whale. Preliminary work was done on developing the user interface.

The final project report mostly follows the format of annual NOPP and ONR project reports. After a formal introduction, the long-term goals, objectives, and approach are presented

20110705022

succinctly. The completed work is then summarized by task and year. The principal accomplishments of the project are listed in the conclusions section together with comments on potential future work based on present findings, ultimately to understand physical effects of sonar interactions with beaked whales.

INTRODUCTION

Mid-frequency (MF) military sonars, with operating frequencies in the 1–10 kHz band, have been implicated in a number of strandings of beaked whales. These strandings have included documented events in Greece in 1996 (Frantzis 1998, D’Spain et al. 2006), in the Bahamas and Madeira in 2000 (NOAA 2001, Cox et al. 2006), and in the Canary Islands in 2002 (Proceed. ECS 2004). Cuvier’s beaked whale (*Ziphius cavirostris*) was especially affected. Some later mass stranding events were also coincident with the use of MF sonar, as in the Haro Strait near Washington State in 2003 (Norman et al. 2004, National Marine Fisheries Service 2005) and off the coasts of Hawaii in 2004 (Southall et al. 2006) and North Carolina in 2005 (Hohn et al. 2006). These later events involved other species, but without the kinds of injuries reported in beaked whales (Freitas 2004, Ketten 2005, Fernández et al. 2005). This history indicates a particular sensitivity of beaked whales to MF sonar. It has motivated a number of studies, including the present one.

Notable hypotheses that have been examined include those of acoustic resonance in the lungs and formation of gas bubbles in potentially super-saturated deep-diving mammals. The first of the hypotheses was eventually discounted (NOAA 2002).

Research since the mid-1990s has focused on sound source characteristics and propagation paths, location and abundance of marine mammal populations, criteria and thresholds for physical and behavioral effects (National Research Council 2000, 2003, 2005), and morphology-based modeling (Aroyan 2001, Krysl et al. 2006, Cranford et al. 2008a). The models are realizations of the finite-element method (Burnett 1987).

It was the ambition of the project summarized here to develop a tool that would enable the community to investigate the physical effects of sonar-induced sound on beaked whales and other marine mammals. This tool would be an interactive online modeling and visualization system. It would enable researchers to predict sonar-induced acoustic fields inside beaked whales as well as inside other marine mammals.

In the event, development of the tool, called the Virtual Beaked Whale, was not completed. However, several other goals were achieved, including synthesis of a morphometric model of a beaked whale. This and work on other tasks, as well as achievements, are summarized below.

The basic form of this report follows that of annual project reports. Long-term goals and scientific and technological objectives are stated succinctly, and the intended approach is summarized. Completed work is then described for each task by year, essentially quoting from the previous annual reports but updating the information too. Main deliverables of the project are listed in the conclusions, which also point to potential future work based on the present findings.

LONG-TERM GOALS

The top-level goal of this project was to build an interactive online modeling and visualization system, called the Virtual Beaked Whale, to enable users to predict mid-frequency sonar-induced acoustic fields inside beaked whales and other marine mammals. Another high-level goal was to acquire new high-resolution morphometric and physical-property data on beaked whales for use in the model. It was hoped that the availability of such a system together with high-quality data would give researchers insight into the nature of sonar interactions with beaked whales, ultimately to introduce objectivity into a public discussion that has been hampered by lack of a scientific approach. It was hoped further that the tool would prove useful in evaluating alternate sonar transmit signals that retain the required information content but with substantially reduced physical effects in beaked whales.

OBJECTIVES

To achieve the long-term goals, a number of scientific and technological objectives were identified. These included the following: extending existing finite-element-method (FEM) code to describe acoustic interactions with structures, and applying this to a virtual beaked whale and mid-sonar frequencies in the range 1–10 kHz; collecting high-resolution morphometric data through computerized tomography (CT) scans on marine mammal specimens, and constructing finite-element models of the anatomy; assigning physical properties of tissues; benchmarking the finite-element code; and incorporating the extended finite-element code and morphometric and physical-property data in an online modeling and visualization system called the Virtual Beaked Whale.

APPROACH

The approach followed an integrated set of six tasks, which are briefly described.

Task 1. Development of a finite-element method to model acoustic interactions: This task was considered as a structural-acoustic problem, in which most tissue groups and surrounding water behave as acoustic fluids and, bony tissues behave as elastic solids. A beaked whale or other marine mammal was to be modeled as a structure represented by its morphometry (Task 2), in which each anatomical part is assigned its own set of physical properties (Task 3).

Task 2. Morphometry and meshing the three-dimensional anatomy: The principal source of morphometric data were CT scans performed at the Woods Hole Oceanographic Institution (WHOI) Computerized Scanning and Imaging (CSI) Facility. Image data on marine mammal specimens were expressed in Digital Imaging and Communications in Medicine (DICOM) format. Amira (Visage Imaging, Inc., San Diego, CA) visualization software was used for segmentation and surface reconstruction. The automatic mesh generation employed tetrahedral elements.

Task 3. Physical properties of tissues: The best available data were to be used to represent the acoustically important properties of mass density, elastic constants, and absorption coefficients for each identified internal organ or other body part.

Task 4. Measuring interactions of acoustic fields with cetacean specimens: In order to test the FEM code (Task 1), measurements were performed of the internal pressure field in selected

tissues in an instrumented common dolphin cadaver, also referred to in this report as a specimen. The specimen was prepared by surgically implanting acoustic sensors in the form of tourmaline pressure gauges; CT-scanned to determine sensor location and morphometry; then acoustically measured at the Naval Surface Warfare Center (NSWC) Carderock Division. A necropsy was performed within hours of the experiment.

Task 5. Testing the FEM model: Rigorous testing was to be performed by comparison with analytic solutions for immersed simple objects. These solutions were developed and numerically realized for acoustically absorptive fluid spheres and solid elastic spheres in a lossy immersion fluid. Numerical solutions for more complicated objects were also identified.

Task 6. Virtual Beaked Whale: This interactive online modeling and visualization system was to be the principal deliverable of the project. It was to incorporate a database with sets of whole-body morphometric data (Task 2) from beaked whales and other species, as well as the respective physical properties of tissues (Task 3). It would also allow users to enter other morphometric and physical-property data directly. The user would be able to specify an essentially arbitrary mid-frequency sonar signal. The output would consist of computed solutions for the internal pressure and displacement fields (Task 1) at user-specified locations.

WORK COMPLETED

Task 1. Development of a finite-element method to model acoustic interactions

2008: Existing finite-element-method (FEM) code to serve as the core of the modeling system was extended in several ways. (1) A perfectly matched layer (Berenger 1994, Turkel and Yefet 1998) was implemented, eliminating extraneous numerical artifacts of wave reflections from the boundary of the computational volume. (2) Frequency-domain elastic elements were realized in code, allowing propagation of shear waves in addition to ordinary, longitudinal acoustic waves in elastic tissues such as bone. (3) Interface elements were added to transfer loads, namely pressure and stress, between acoustic and elastic elements, which was essential for representing interaction effects within the animal model. (4) A ten-node tetrahedral element was implemented in the code allowing for quadratic interpolation of the basic fields. It was noted that quadratic elements have better numerical properties than linear elements, including that of numerical dispersion, or wave-speed effects due to the finite size of elements, as well as permitting use of fewer nodal points to achieve a predefined accuracy.

2009: An essential and intricate computational problem was addressed. This concerned the construction of software capable of efficiently solving structural acoustic problems with millions of degrees of freedom. This was required to solve problems involving acoustic interactions with heterogeneous structures and generic interfaces, e.g., marine mammals in their natural state of immersion. The associated FEM code, generically called the finite-element solver, was now capable of solving general structural-acoustic problems. This incorporated earlier work implementing a perfectly matching layer, realizing acoustic and elastic elements and interface elements to transfer loads between these, and implementing a ten-node tetrahedral element for quadratic interpolation of the basic fields.

Task 2. Morphometry and meshing the three-dimensional anatomy

2008: Work was completed on several operations necessary for representing the animal model in a three-dimensional computational space. Anatomical realizations by Amira were interfaced with the basic meshing software and FEM software. This enabled a larger computational volume to be represented where the perfectly matching layer was defined.

The meshing process is illustrated in Fig. 1 using morphometric data derived from CT scans on a 142-cm-long common dolphin specimen. Finite-element models based on tetrahedral elements are shown in Figs. 2–4. The scan was performed at 8-mm intervals, hence with 8-mm slice thickness.

A second specimen, a 138-cm-long common dolphin, was CT-scanned at the WHOI CSI Facility at much higher resolution using 1-mm-thick slices. CT data on a living bottlenose dolphin were received from the U.S. Navy Marine Mammal Program.

Images of tissues were also identified by tissue group in an operation called labeling. In the case of the same 142-cm-long common dolphin, upper respiratory and nearby tissues are labeled in Fig. 5. Missing lung tissue, due to the resolution of the 8-mm scan, are also indicated.

2009: Another essential and intricate computational problem was addressed. This concerned the creation of finite-element models that conform to tissue interfaces. This required the use of unstructured meshes as opposed to rectangular, Cartesian grids. CT images had to be segmented; surfaces between different, contiguous tissues had to be triangulated; and the encapsulated volumes had to be filled with volumetric elements, which were tetrahedral for the sake of computational accuracy and efficiency. These volumetric elements were geometrically constrained to avoid extreme acute and obtuse shapes. It is noted that commercially available software, such as Amira, was powerful for segmentation and surface reconstruction, but inadequate for automatic generation of three-dimensional meshes. In addition, it could not generate the meshes needed for defensible acoustic calculations, such as the creation of perfectly matched layers (PML), among other things. Using customized software, three-dimensional visualizations and/or meshes were prepared for each of three common dolphins, designated D_del40, D_del42, and D_del52. The specimen of D_del52 was used in the experiment described under Task 4. In addition, visualization and meshing of a minke whale head was commenced in anticipation of modeling a virtual beaked whale.

2010: The principal deliverable of the project, the Virtual Beaked Whale as described under Task 6, required a morphometric model for a beaked whale. Potential sources of such data included gross anatomical measurements on a number of stranded beaked whales and computerized tomographic (CT) scans of the heads of a very few, different beaked whale specimens. Adult beaked whales are simply too large for ordinary CT-scanning. To remedy this shortcoming, a synthetic model was developed based on the following sources of data: (i) head of a Cuvier's beaked whale (*Ziphius cavirostris*), a sub-adult male, total length 4 m, mass 730 kg, derived from a stranding on Cape Cod at Sandy Beach, Cohasset, MA, on 4 April 2006, with euthanization by the Cape Cod Stranding Network, delivered to WHOI for dissection, and head CT-scanned fresh on 5 April 2006 at WHOI, and (ii) body of a harbor porpoise (*Phocoena*

phocoena), an adult male, length 105 cm, mass 22.1 kg, dead of natural causes on 22 February 2010, found in Wellfleet, MA, delivered to WHOI by the International Fund for Animal Welfare (IFAW), and scanned fresh the following day, 23 February 2010, at WHOI. There is a presumption that the anatomy of the harbor porpoise body resembles that of a Cuvier's beaked whale, at least to within a scaling factor. The corresponding morphometric data were synthesized by reducing the head of the beaked whale specimen to the body of the harbor porpoise, rather than by enlarging the body of the harbor porpoise to the head of the beaked whale. More particularly, the head of the beaked whale was scaled and stitched to the body of the harbor porpoise within the Amira environment.

The process of synthesizing the beaked whale model is illustrated in Figs. 6–8. The basic material consists of CT images of anatomical cross sections, as in Fig. 6. These were segmented, a process in which tissues are labeled, allowing automatic linking in volumetric rendering across slices. Ultimately this enables sagittal and coronal views to be formed, as in Fig. 7, as well as transparent views, as in Fig. 8.

Prior to modeling the sonar-induced fields, the synthetic beaked whale would be scaled to full beaked-whale size. In the present case of Cuvier's beaked whale, the overall length would be of order 4–8 m.

2011: The synthesis process was completed and publication was initiated on the CSI website [<http://csi.whoi.edu/>].

Task 3. Physical properties of tissues

2009: The subject of physical properties of marine mammal tissue was discussed extensively. It was clear that current knowledge of physical properties was mostly derived from *ex situ* measurements rather than the more desirable *in vivo* measurements. It was also appreciated that the physical properties of some tissues are influenced by pressure, e.g., the lungs and other air-containing tissues, by both pressure and temperature, as in the case of the melon.

2010: Physical properties of beaked whale tissue: This was a continued subject of discussion. The basic problem was the lack of data, further exacerbated by the use of frozen and thawed tissue samples for the few measurements that have been undertaken for beaked whale tissue. An unexpected source of direct, *ex situ* measurements on fresh tissue was identified. This was a series of measurements of the longitudinal-wave sound speed performed by D. Chu and A. Lavery on tissue samples extracted from the freshly stranded Cuvier's beaked whale described above under Task 2. Measurements were performed with a unique apparatus (Chu and Wiebe 2005), which had earlier been applied to zooplankton (Chu et al. 2000, 2003; Wiebe et al. 2010). The measured beaked whale tissues included samples from the ventral, medial, and dorsal parts of the melon; blubber; fat; and muscle. The Chu and Lavery data were not completely analyzed following their collection on 6 April 2006, and were not published.

Gas volume conformational changes in beaked whales: The volume of gas contained within air spaces of a diving and ascending odontocete will vary depending upon depth, functional use, and compliance of the surrounding tissues. The dynamic relationship between gas volumes and

ambient pressure is well understood, and can be used to make general assumptions about the total gas volume held within the whale at any depth relative to the total volume held at surface level. However, biological material is not uniform and therefore variations in compliance must be accounted for when examining pressure-volume relationships. The gas-containing organs can have a range of compliances depending upon the structure of the interstitial and surrounding tissues. Lungs, for example, are highly elastic, but have some stretch constraints related to their internal construction. The jointed ribs of odontocetes allow additional flexibility for lung collapse compared with terrestrial animals. The cartilage surrounding the larynx and trachea, particularly the complete circular rings found in whales, makes it stiffer than the lungs, but more pliant than the skull. Cranial bony sinuses are rigid and could crack under pressure changes if the ostia allowing gas exchange are insufficient or blocked. Odontocetes have thus evolved air sacs outside the skull that are free of the constraints of rigid bony walls. These air sacs are probably even more elastic than lungs, particularly as they have highly folded external contours and no tissues crossing through their lumen. At extreme depths, it is likely that these spaces collapse as they are completely evacuated of gas. Some species of deep diving beaked whales have evolved reduced or absent air sacs, probably through selection against these non-functional spaces at full collapse, which become liability for infections. There are several major functional conditions under which odontocete respiratory spaces may undergo conformational changes during a dive: breathing, sound production, hearing, and valsalva. It is clear that current knowledge of beaked whale anatomy is inadequate to predict gas volume conformational changes with depth and function.

2011: An attempt was made to survey the literature on acoustically significant properties of cetacean tissues, with summary in Table I. These properties are allowed to subsume the conventional physical properties of mass density, sound speed, compressibility, and their pressure and temperature dependences; anatomical properties, including morphology and topology; and biochemistry, including molecular composition. The source literature is diverse, reflecting the many interesting aspects of cetacean tissue properties. These span such issues as buoyancy with respect to temperature and pressure, recognizing that lipids undergo a phase change within the ordinary diving range of sperm whales and other odontocetes; role of blubber; audiology; and sound generation, including echolocation. The importance of lipid composition with tissue location is appreciated apropos of sound propagation (Koopman et al. 2003, 2006; Duggan et al. 2009). Duggan et al. (2009) noted the relationship of carbon chain length to sound speed, which is inverse (Gouw and Vlugter 1967, Hustad et al. 1971).

It is observed from the table that the measurements and reported data are quite limited. Notable exceptions are works dating from Soldevilla et al. (2005), which attempt to represent the physical properties of cetacean tissues in a comprehensive manner that would be self-sufficient for modeling purposes. In Soldevilla et al. (2005) and some other studies, the mass density of tissues was assumed to be accessible through the X-ray absorption measurements that are fundamental to computed tomography (CT), and conversion from Hounsfield units to units of mass density were effected through calibrations that can be traced to measurements on phantom targets of known mass density. The represented acoustic properties also included absorption.

Determination of the physical properties of cetacean tissues represents an outstanding problem that has attracted attention and funding. Thus far, tools or methods to accomplish such

measurements *in vivo* are wanting. Inference of tissue properties by a combined program of measurement of sonar-induced fields inside instrumented specimens and modeling may be the most effective approach. Certainly the issue of data quality is important when justifying conclusions being drawn from modeling studies about the physical effects of sonar.

Task 4. Measuring interactions of acoustic fields with cetacean specimens

2008: A series of tests were performed on sensors to be used in the acoustic experiments with instrumented marine mammal specimens at NSWC. These tests established that tourmaline sensors typically used at shock-pressure levels can also be used at sub-shock levels, and that new Lenz-effect transducers can generate powerful acoustic signals in the upper part of the mid-frequency sonar band. Experience was gained in configuring the facility for experiments with marine mammal specimens through measurements performed at the same facility on a 30-kg pig carcass. This carcass was instrumented through surgical implantation of tourmaline sensors, and used in acoustic tests in preparation for the anticipated marine mammal specimen experiments.

2009: During early February 2009, the first experiment with a marine mammal specimen was performed at NSWC Carderock Division. The specimen was that of a young adult male common dolphin (*Delphinus delphis*), 119 kg, 211-cm total length, that had stranded and died on a Cape Cod beach two months previously. In the interim the specimen, designated D_del52, was stored at WHOI in a freezer at -20°C. CT scans were obtained in the frozen state and following thawing to assess overall tissue condition, indicated in Fig. 9(a). Tourmaline pressure gauges, Fig. 9(b), were surgically implanted in the nares, left lung, right lung, external right lung, melon, along right ear, epaxial muscle near the dorsal fin, and rectal abdomen, with locations summarized in Table II. CT scans were repeated, Fig. 10, to determine the precise anatomical locations of the eight gauges, visualized in detail in Figs. 11 and 12. The specimen was transported in a chilled state to NSWC by car.

On 3 February acoustic calibration data were collected on the external tourmaline gauges mounted on the suspension frame ensonified with a pair of International Transducer Corporation (Santa Barbara, CA) ITC-1032 transducers arranged in a dipole-like configuration with a 15-cm rod separating the two.

On 4 February the specimen was suspended within a PVC-pipe frame, Fig. 13, and immersed in the fresh water Test Explosion Pond, Figs. 14–16, with specimen at 2-m depth. It was exposed to multiple ensonifications by a single ITC-1032 spherical transducer, with measured source levels described in Table III. This was excited at each of three frequencies: 5, 7, and 10 kHz, by a 20-cycle sinusoidal burst with smooth rise and fall over two cycles, for each of three source locations: in front of the rostrum, and successively on the right and left sides of the specimen, with but different fore-aft and up-down locations. The detailed locations are described in Table IV. Data were recorded simultaneously on 15 channels from the six external tourmaline gauges, eight implanted gauges, and source transducer, over a total of 5 s for each frequency and source location, with 4-Hz pulse repetition frequency. Each signal was amplified by a PCB model 422E01 inverting-charge amplifier and digitized at 100 kHz. Overviews of the acoustic data at 7 kHz are presented in Fig. 17 for the source on the right side of the specimen, and in Fig. 18 for the source in front of the specimen. Details from Fig. 18 are shown in Fig. 19 together with the

respective results of band-pass and matched filtering of the several signals. Corresponding data at 5 and 10 kHz are shown in Fig. 20 together with the respective processing results. Noise data were also collected passively, without source excitation, at the end of each series.

After the experiment, the specimen was removed from the suspension frame and transported by car to the Walter Reed Army Institute for Research (WRAIR), where a necropsy was performed, led by Dr. D. R. Ketten. Tissues were observed for trauma and samples collected for histological analysis. A WHOI CSI-Scanning and Necropsy Report was prepared.

The acoustic data were comprehensively reviewed within the MATLAB environment. Noise was prominent at 60 Hz and at sub-hertz frequencies, which is evident in the total signals presented in Figs. 17 and 18. The sub-hertz noise was necessarily non-stationary owing to the short, 5-s data collection periods. Both noise types were removed by digital band-pass filtering with a bandwidth equal to 10% of the center frequency of the transmit signal. The effects of such filtering supplemented by matched filtering are shown in Fig. 21 for the case of the source in front of the specimen and transmit signal centered at 7 kHz. Details of the processing are also shown in Figs. 22 and 23. Qualitative conclusions were supplemented by a detailed quantitative analysis, with results presented in Table V.

2010: In the experiment performed on the instrumented specimen of a young adult male common dolphin (*Delphinus delphis*) at NSWC on 4 February 2009, sonar-induced internal fields were measured with tourmaline gauges. These are more commonly used to measure high-amplitude, e.g., blast fields (Rogers 1997). However, they are evidently suitable for measuring low-amplitude, sub-shock fields too. During the experiment, the signals at the output of the gauges were amplified by PCB 422 in-line preamplifiers, providing a voltage gain of 100. Earlier performance measurements of tourmaline gauges were refined and extended. In particular, two tourmaline gauges together with the mentioned preamplifiers were calibrated using a calibrated Brüel & Kjær (Nærum, Denmark) B&K 8103 laboratory hydrophone.

2011: Analysis of the experiment was completed, and a manuscript was prepared and submitted for publication (Foote et al., submitted).

The tourmaline sensors first used in sub-shock measurements in 2008, and reported above, were documented in preliminary form (Morales et al. 2011).

Task 5. Testing the FEM model

2008: Analytic solutions for the acoustic interaction of plane acoustic waves with an immersed, absorbing, fluid sphere were developed and rendered in code for use in validating the FEM code. These solutions were realized numerically (Foote 2007a,b) for a 50-mm-diameter sphere ensonified at 10 and 100 kHz. The immersion medium was represented as water of mass density 1000 kg/m^3 , sound speed 1500 m/s, and variable absorption in the range 0–10 dB/wavelength. The sphere was represented as a fluid with variable mass density over the range 500–2000 kg/m^3 to achieve density contrasts with water of 0.5–2, variable sound speed over 750–3000 m/s to achieve sound speed contrasts with water of 0.5–2, and variable absorption coefficient over 0–10 dB/wavelength. The pressure and displacement fields were computed along the sphere axis, as

defined by direction of propagation of the incident wave; transverse to this axis from center; and along the surface from the forward to reverse directions.

2009: The FEM code described in Task 1 was to be benchmarked through a series of test computations. (1) Surface fields on the spherical shape due to plane-wave ensonification were computed for each of two boundary conditions: pressure-release and rigid, for wavenumber-radius products over the range 0-15. Farfield backscattering cross sections were computed on the basis of the surface fields and compared with known solutions. (2) Plane-wave-induced pressure fields in a fluid sphere with relative sound speed 0.8 and mass density equal to that of the immersion medium were computed for wavenumber-radius products over the range 0-15. The reflectivity coefficient was computed on the basis of the surface field and compared with the solution due initially to Anderson (1950). (3) Internal displacement and stress fields in a solid elastic sphere were computed. The farfield scattering form function was computed as a function of frequency for comparison with numerical results due initially to Faran (1951). Relative errors were estimated for different mesh sizes relative to the acoustic wavelength. (4) Internal displacement and stress fields induced by spherical waves incident on elastic spherical and cylindrical shells were computed.

Analytic solutions for the acoustic interaction of both plane and spherical acoustic waves in an absorbing fluid sphere immersed in a lossy immersion fluid were developed and rendered in code for use in validating the FEM code. These solutions were realized numerically for a 50-mm-diameter sphere ensonified at 10 and 100 kHz. The immersion medium was represented as water of mass density 1000 kg/m^3 , sound speed 1500 m/s, and variable absorption in the range 0-10 dB/wavelength. The sphere was represented as a fluid with variable mass density over the range 500-2000 kg/m^3 to achieve density contrasts with water of 0.5-2, variable sound speed over 750-3000 m/s to achieve sound speed contrasts with water of 0.5-2, and variable absorption coefficient of 0 or 10 dB/wavelength. The pressure and displacement fields were computed along the sphere axis, as defined by direction of propagation of the incident wave; transverse to this axis from center; and along the surface from the forward to reverse directions. In a special additional case, that of a focusing sphere with fluid mass density 1900 kg/m^3 and sound speed 857 m/s, the fields were also computed with high precision at selected points for detailed comparison and assessment of computational accuracy, with results in Fig. 24. Preliminary documentation is contained in three abstracts (Foote 2007a,b; Foote and Francis 2008).

A separate solution for the pressure and particle-velocity fields in a thin spherical shell due to an external point source is presented in Fig. 25.

2010: Work designed for benchmarking computer code that solves the full-diffraction wave equation inside generally irregular and heterogeneous bodies was continued. The analytic solution was generalized to the case of point sources in the nearfield of absorbing fluid spheres in a lossy fluid immersion medium. Detailed results suitable for benchmarking are presented in Tables VI and VII. Tests were also performed using boundary-element and finite-element codes (Foote et al. 2009, 2010).

Analytic solutions for the acoustic interaction of both plane and spherical acoustic waves in an absorbing solid elastic sphere immersed in a lossy immersion fluid were also developed and

rendered in code. These solutions were realized numerically for a 50-mm-diameter sphere of high-density polyethylene ensonified by a plane wave of amplitude 1 Pa at 100 kHz. The immersion medium was represented as water of mass density 1000 kg/m^3 , sound speed 1500 m/s, with no absorption and with longitudinal-wave absorption 0.4 dB/wavelength and transverse-wave absorption 1.2 dB/wavelength. The radial stress and radial displacement fields were computed along the sphere axis, as defined by direction of propagation of the incident wave, with results in Fig. 26. Preliminary documentation is contained in an abstract (Foote et al. 2010).

Task 6. Virtual Beaked Whale

2008: Visualization routines were developed to return data from the FEM system and display these on a webpage. This system was operational in a pilot mode and was being used internally. Significant achievements included specification of the sonar frequency and direction of the incident plane wave, and development of a client-server system that displayed the computational results in the form of pressure fields in user-defined cross sections of the computational domain. The client-server system is responsible for passing data among the different components of the simulation environment, namely meshing, preprocessing, and FEM-analysis programs. The visualization system was based in MATLAB, and was capable of operating with meshes of up to two million elements. A new, successor system was to be capable of operating with meshes with more than 20 million elements.

Work was commenced on developing a graphical user interface for the Virtual Beaked Whale. Preliminary results are shown in Fig. 27.

2009: A user group composed of colleagues from the international bioacoustics community was defined for testing the Virtual Beak Whale when in a more advanced state.

2010: Modeled results for the pressure magnitude on the skeleton of the common dolphin specimen D_del42 are shown in Fig. 28.

A substantial computing platform was acquired and configured to support the Virtual Beaked Whale. This was an HP ProLiant DL585 G6 server, with four six-core processors and four 500-GB SATA disks. A user's guide for operating the Virtual Beaked Whale was outlined.

CONCLUSIONS

Developing an interactive online modeling and visualization system to predict sonar-induced acoustic fields inside beaked whales as well as inside other marine mammals is a formidable task. It was the overarching goal of the project to effect this system, but it was not completed. However, the essential composition of this system was specified in detail, recognizing that it would be necessary to solve several tens of millions of equations simultaneously.

A synthetic model of Cuvier's beaked whale was developed based on CT scans of the head of a freshly dead Cuvier's beaked whale and CT scans of the body of a harbor porpoise. These data, in segmented form, are available from the Woods Hole Oceanographic Institution (WHOI) Computerized Scanning and Imaging (CSI) Facility website [<http://csi.whoi.edu/>].

Source literature reporting physical property values of cetacean tissues or closely related topics has been summarized.

Tourmaline sensors can be used to measure relatively weak, sub-shock acoustic pressures.

Sonar-induced acoustic pressure fields inside a common dolphin cadaver have been measured. Both amplitudes and times of flight have been measured.

Analytic models have been developed for benchmarking FEM code based on the interaction of plane harmonic pressure waves with lossy fluid and solid elastic spheres.

In the future, experimental measurements of sonar-induced acoustic fields inside instrumented marine mammal cadavers may be useful for investigating sound transmission pathways and for inferring acoustic properties of ensonified tissues.

ACKNOWLEDGEMENTS

The contributions of J. A. Clark, deceased, are gratefully acknowledged. The work of the CoPIs G. Feijoo, M. C. Hastings, J. S. Reidenberg, and K. Ryc is acknowledged. W. H. Lewis and other colleagues at NSWC are thanked for participating in the experiment. D. R. Ketten, J. Arruda, and S. Cramer are thanked for diverse contributions. M. Parmenter is thanked for editorial assistance. The support of J. Eckman and M. Weise is gratefully acknowledged. This project was supported by NOPP through ONR Award No. N000140710992.

PROJECT PUBLICATIONS

G. Feijoo and K. G. Foote, "An acoustic finite-element model to study sonar interactions with marine mammals (A)," *J. Acoust. Soc. Am.* **124**, 2466 (2008).

K. G. Foote, "Interaction of an inhomogeneous acoustic plane wave with a fluid sphere: Analytical solution (A)," *J. Acoust. Soc. Am.* **121**, 3040 (2007a).

K. G. Foote, "Internal field in an immersed, absorbing fluid sphere excited by a plane acoustic wave (A)," *J. Acoust. Soc. Am.* **122**, 3033–3034 (2007b).

K. G. Foote, "Mid-frequency sonar interactions with beaked whales (A)," in *ONR Marine Mammal Program Review, 7–10 December 2009 Abstracts* (Office of Naval Research, 2009), pp. 140-141.

K. G. Foote and D. T. I. Francis, "Pressure and displacement fields inside an absorbing fluid sphere ensonified by a plane harmonic wave (A)," *J. Acoust. Soc. Am.* **124**, 2517 (2008).

K. G. Foote, D. T. I. Francis, and M. Zampolli, "Pressure and displacement fields inside an absorbing fluid sphere ensonified by a point acoustic source: Comparison of analytic and numerical solutions (A)," *J. Acoust. Soc. Am.* **126**, 2244 (2009).

K. G. Foote, D. T. I. Francis, M. Zampolli, and T. van Zon, "Sonar-induced strains and stresses in an absorbing solid elastic sphere (A)," *J. Acoust. Soc. Am.* **127**, 1952 (2010).

K. G. Foote, M. C. Hastings, D. R. Ketten, Y.-T. Lin, J. S. Reidenberg, and K. Rye, "Sonar-induced pressure fields in a common dolphin," (submitted 2011).

J. Morales, A. Kale, and M. Hastings, "Performance of tourmaline hydrophones at low- and midfrequencies (A)," *J. Acoust. Soc. Am* **129**, 2343 (2011).

ADDITIONAL CITED REFERENCES

R. G. Ackman, J. H. Hingley, C. A. Eaton, V. H. Logan, and P. H. Odense, "Layering and tissue composition in the blubber of the northwest Atlantic sei whale (*Balaenoptera borealis*)," *Can. J. Zool.* **53**, 1340–1344 (1975).

V. C. Anderson, "Sound scattering from a fluid sphere," *J. Acoust. Soc. Am.* **22**, 426–431 (1950).

J. L. Aroyan, "Three-dimensional modeling of hearing in *Delphinus delphis*," *J. Acoust. Soc. Am.* **110**, 3305–3318 (2001).

J.-P. Berenger, "A perfectly matched layer for the absorption of electromagnetic waves," *J. Comput. Phys.* **114**, 185–200 (1994).

J. Blomberg and B. N. Jensen, "Ultrasonic studies on the head oil of the North Atlantic pilot whale (*Globicephala melaena melaena*) (L)," *J. Acoust. Soc. Am.* **60**, 755–758 (1976).

J. Blomberg and L.-E. Lindholm, "Variations in lipid composition and sound velocity in melon from the North Atlantic pilot whale, *Globicephala melaena melaena*," *Lipids* **11**(2), 153–156 (1976).

D. S. Burnett, *Finite Element Analysis: From Concepts to Applications* (Addison-Wesley, Reading, MA, 1987), 844 pp.

D. Chu and P. H. Wiebe, "Measurements of sound-speed and density contrasts of zooplankton in Antarctic waters," *ICES J. Mar. Sci.* **62**, 818–831 (2005) [doi: 10.1016/j.icesjms.2004.12.020].

D. Chu, P. Wiebe, and N. Copley, "Inference of material properties of zooplankton from acoustic and resistivity measurements," *ICES J. Mar. Sci.* **57**, 1128–1142 (2000) [doi: 10.1006/jmsc.2000.0800].

D. Chu, P. H. Wiebe, N. J. Copley, G. L. Lawson, and V. Puvanendran, "Material properties of North Atlantic cod eggs and early-stage larvae and their influence on acoustic scattering," *ICES J. Mar. Sci.* **60**, 508–515 (2003) [doi: 10.1016/S1054-3139(03)00047-X].

M. R. Clarke, "Function of the spermaceti organ of the sperm whale," *Nature* **228**, 873–874 (1970).

M. R. Clarke, "Structure and proportions of the spermaceti organ in the sperm whale," J. Mar. Biol. Ass. U.K. **58**, 1–17 + 2 plates (1978a).

M. R. Clarke, "Physical properties of spermaceti oil in the sperm whale," J. Mar. Biol. Ass., U.K. **58**, 19–26 (1978b).

M. R. Clarke, "Buoyancy control as a function of the spermaceti organ in the sperm whale," J. Mar. Biol. Ass. U.K. **58**, 27–71 (1978c).

M. R. Clarke, "Production and control of sound by the small sperm whales, *Kogia breviceps* and *K. sima* and their implications for other Cetacea," J. Mar. Biol. Ass. U.K. **83**, 241–263 (2003).

T. M. Cox, T. J. Ragen, A. J. Read, E. Vos, R. W. Baird, K. Balcomb, J. Barlow, J. Caldwell, T. Cranford, L. Crum, A. D'Amico, G. D'Spain, A. Fernández, J. Finneran, R. Gentry, W. Gerth, F. Gulland, J. Hildebrand, D. Houser, T. Hullar, P. D. Jepson, D. Ketten, C. D. MacLeod, P. Miller, S. Moore, D. C. Mountain, D. Palka, P. Ponganis, S. Rommel, T. Rowles, B. Taylor, P. Tyack, D. Wartzok, R. Gisiner, J. Mead, and L. Benner, "Understanding the impacts of anthropogenic sound on beaked whales," J. Cetacean Res. Manage. **7**, 177–187 (2006).

T. W. Cranford, P. Krysl, and J. A. Hildebrand, "Acoustic pathways revealed: Simulated sound transmission and reception in Cuvier's beaked whale (*Ziphius cavirostris*)," Bioinspir. Biomim. **3**, 10 pp. (2008a) [doi: 10.1088/1748-3182/3/1/016001].

T. W. Cranford, M. F. McKenna, M. S. Soldevilla, S. M. Wiggins, J. A. Goldbogen, R. E. Shadwick, P. Krysl, J. A. St. Legcr, and J. A. Hildebrand, "Anatomic geometry of sound transmission and reception in Cuvier's beaked whale (*Ziphius cavirostris*)," Anat. Rec. **291**, 353–378 (2008b).

CSI: Computerized Scanning and Imaging Facility of Woods Hole Oceanographic Institution, Woods Hole, MA. Available online at <http://csi.whoi.edu/> (Last viewed 17 June 2011).

G. L. D'Spain, A. D'Amico, and D. M. Fromm, "Properties of underwater sound fields during some beaked whale mass stranding events," J. Cetacean Res. Manage. **7**, 223–238 (2006).

Z. P. Z. Duggan, H. N. Koopman, and S. M. Budge, "Distribution and development of the highly specialized lipids in the sound reception systems of dolphins," J. Comp. Physiol. B **179**, 783–798 (2009).

J. J. Faran, Jr., "Sound scattering by solid cylinders and spheres," J. Acoust. Soc. Am. **23**, 405–418 (1951).

A. Fernández, J. F. Edwards, F. Rodriguez, A. Espinosa de los Monteros, P. Herraiez, P. Castro, J. R. Jaber, V. Martin, and M. Arbelo, "'Gas and fat embolic syndrome' involving a mass stranding of beaked whales (family Ziphiidae) exposed to anthropogenic sonar signals," Veterinary Pathology **42**, 446–457 (2005).

- A. Frantzis, "Does acoustic testing strand whales?" *Nature* **392**, 29 (1998).
- L. Freitas, "The stranding of three Cuvier's beaked whales *Ziphius cavirostris* in Madeira archipelago – May 2000," in *Proceedings of the Workshop on Active Sonar and Cetaceans, European Cetacean Society's 17th Annual Conference, Las Palmas, Canary Islands, 8 March 2003*, edited by P. G. H. Evans and L. A. Miller (European Cetacean Society Newsletter, No. 42-Special Issue, 2004), pp 28–32.
- J. C. Goold and M. R. Clarke, "Sound velocity in the head of the dwarf sperm whale, *Kogia sima*, with anatomical and functional discussion," *J. Mar. Biol. Ass., U.K.* **80**, 535–542 (2000).
- I. R. T. H. Gouw and I. R. J. C. Vlugter, "Physical properties of triglycerides III: Ultrasonic sound velocity," (German translation) *Fette, Seifen, Anstrichmittel* **69**(3), 159-164 (1967) [doi: 10.1002/lipi.19670690301].
- A. A. Hohn, D. S. Rotstein, C. A. Harms, and B. L. Southall, "Report on marine mammal unusual mortality event UMESE0501Sp: Multispecies mass stranding of pilot whales (*Globicephala macrorhynchus*), minke whale (*Balaenoptera acutorostrata*), and dwarf sperm whales (*Kogia sima*) in North Carolina on 15-16 January 2005," NOAA Technical Memorandum NMFS-SEFSC-537, 222 pp. (2006).
- S. Huggenberger, M. A. Rauschmann, T. J. Vogl, and H. H. A. Oelschläger, "Functional morphology of the nasal complex in the harbor porpoise (*Phocoena phocoena* L.)," *Anat. Rec.* **292**, 902–920 (2009).
- G. O. Hustad, T. Richardson, W. C. Winder, and M. P. Dean, "Acoustic properties of some lipids," *Chem. Phys. Lipids* **7**(1–2), 61–74 (1971) [doi: 10.1016/0009-3084(71)90020-X].
- H. Karol, C. Litchfield, D. K. Caldwell, and M. C. Caldwell, "Compositional topography of melon and spermaceti organ lipids in the pygmy sperm whale *Kogia breviceps*: Implications for echolocation," *Mar. Biol.* **47**, 115–123 (1978).
- D. K. Ketten, "Beaked whale necropsy findings for strandings in the Bahamas, Puerto Rico, and Madeira, 1999–2002," Woods Hole Oceanographic Institution Technical Report, WHOI-2005-09, 38 pp. (2005). Available online at <http://www.whoi.edu/csi/images/WHOI-2005-09.pdf> (Last viewed 17 June 2011).
- M. Klinowska, *Dolphins, Porpoises and Whales of the World. The IUCN Red Data Book* (IUCN, Gland, Switzerland and Cambridge, U.K., 1991) viii + 429 pp.
- H. N. Koopman, S. M. Budge, D. R. Ketten, and S. J. Iverson, "Topographical distribution of lipids inside the mandibular fat bodies of odontocetes: Remarkable complexity and consistency," *IEEE J. Ocean. Eng.* **31**, 95–105 (2006).

H. N. Koopman, S. J. Iverson, and A. J. Read, "High concentrations of isovaleric acid in the fats of odontocetes: Variation and patterns of accumulation in blubber vs. stability in the melon," *J. Comp. Physiol. B* **173**, 247–264 (2003).

P. Krysl, T. W. Cranford, S. M. Wiggins, and J. A. Hildebrand, "Simulating the effect of high-intensity sound on cetaceans: Modeling approach and a case study for Cuvier's beaked whale (*Ziphius cavirostris*)," *J. Acoust. Soc. Am* **120**, 2328–2339 (2006).

C. Litchfield and A. J. Greenberg, "Comparative lipid patterns in the melon fats of dolphins, porpoises and toothed whales," *Comp. Biochem. Physiol.* **47B**, 401–407 (1974).

C. Litchfield, A. J. Greenberg, D. K. Caldwell, M. C. Caldwell, J. C. Sipos, and R. G. Ackman, "Comparative lipid patterns in acoustical and nonacoustical fatty tissues of dolphins, porpoises and toothed whales," *Comp. Biochem. Physiol.* **50B**, 591–597 (1975).

C. Lockyer, "Body composition of the sperm whale, *Physeter catodon*, with special reference to the possible functions of fat depots," *Rit Fiskideildar. [J. Mar. Res. Inst., Reykjavik]* **12**(2), 1–24 (1991).

M. F. McKenna, J. A. Goldbogen, J. St. Leger, J. A. Hildebrand, and T. W. Cranford, "Evaluation of postmortem changes in tissue structure in the bottlenose dolphin (*Tursiops truncatus*)," *Anat. Rec.* **290**, 1023–1032 (2007).

R. J. Morris, "The lipid structure of the spermaceti organ of the sperm whale (*Physeter catodon*)," *Deep-Sea Res.* **20**, 911–916 (1973).

R. J. Morris, "Further studies into the lipid structure of the spermaceti organ of the sperm whale (*Physeter catodon*)," *Deep-Sea Res.* **22**, 483–489 (1975).

National Marine Fisheries Service, "Assessment of acoustic exposures on marine mammals in conjunction with *USS Shoup* active sonar transmissions in the Eastern Strait of Juan de Fuca and Haro Strait, Washington, 5 May 2003," Office of Protected Resources, 13 pp. (2005). Available online at <http://www.nmfs.noaa.gov/pr/pdfs/acoustics/assessment.pdf> (Last viewed 17 June 2011).

National Research Council (NRC), *Marine Mammals and Low-Frequency Sound* (National Academies Press, Washington, D.C., 2000), 160 pp.

National Research Council (NRC), *Ocean Noise and Marine Mammals* (National Academies Press, Washington, D.C., 2003), 204 pp.

National Research Council (NRC), *Marine Mammal Populations and Ocean Noise: Determining When Noise Causes Biologically Significant Effects* (National Academies Press, Washington, D.C., 2005), 142 pp.

NOAA, "Joint interim report Bahamas marine mammal stranding event of 15-16 March 2000," NOAA, December 2001, 66 pp. Available online at http://www.nmfs.noaa.gov/pr/pdfs/health/stranding_bahamas2000.pdf (Last viewed 17 June 2011).

NOAA, "Report of the workshop on acoustic resonance as a source of tissue trauma in cetaceans. April 24 and 25, 2002 Silver Spring, MD," NOAA, November 2002, 19 pp. Available online at <http://www.nmfs.noaa.gov/pr/pdfs/acoustics/cetaceans.pdf> (Last viewed 17 June 2011).

S. A. Norman, S. Raverty, S. B. McLellan, A. Pabst, D. Ketten, M. Fleetwood, J. K. Gaydos, B. Norberg, L. Barre, T. Cox, B. Hanson, and S. Jeffries, "Multidisciplinary investigation of stranded harbor porpoises (*Phocoena phocoena*) in Washington State with an assessment of acoustic trauma as a contributory factor (2 May–2 June 2003)," U.S. Dept. of Commerce, NOAA Technical Memorandum NMFS-NWR-34, 120 pp. (2004).

K. S. Norris and G. W. Harvey, "Sound transmission in the porpoise head," *J. Acoust. Soc. Am.* **56**, 659–664 (1974).

D. A. Parry, "The structure of whale blubber, and a discussion of its thermal properties," *Q. J. Microsc. Sci.* **s3-90**(9), 13–25 + 1 plate (1949).

Proceedings of the Workshop on Active Sonar and Cetaceans, European Cetacean Society's 17th Annual Conference, Las Palmas, Canary Islands, 8 March 2003, edited by P. G. H. Evans and L. A. Miller (European Cetacean Society Newsletter, No. 42-Special Issue, 2004), 84 pp.

P. H. Rogers, "Electroacoustic devices," in *The Electrical Engineering Handbook, Second Edition*, edited by Richard C. Dorf (CRC Press, Boca Raton, FL, 1997), Chap. 46, pp. 1147–1153.

M. S. Soldevilla, M. F. McKenna, S. M. Wiggins, R. E. Shadwick, T. W. Cranford, and J. A. Hildebrand, "Cuvier's beaked whale (*Ziphius cavirostris*) head tissues: Physical properties and CT imaging," *J. Exp. Biol.* **208**, 2319–2323 (2005).

B. L. Southall, R. Braun, F. M. D. Gulland, A. D. Heard, R. W. Baird, S. M. Wilkin, and T. K. Rowles, "Hawaiian melon-headed whale (*Peponocephala electra*) mass stranding event of July 3-4, 2004," NOAA Technical Memorandum NMFS-OPR-31, 73 pp. (2006).

E. Turkel and A. Yefet, "Absorbing PML boundary layers for wave-like equations," *Appl. Numer. Math.* **27**, 533–557 (1998).

U. Varanasi, H. R. Feldman, and D. C. Malins, "Molecular basis for formation of lipid sound lens in echolocating cetaceans," *Nature* **255**, 340–343 (1975).

Y. Wedmid, C. Litchfield, R. G. Ackman, J. C. Sipos, C. A. Eaton, and E. D. Mitchell, "Heterogeneity of lipid composition within the cephalic melon tissue of the pilot whale (*Globicephala melaena*)," *Biochim. Biophys. Acta* **326**, 439–447 (1973).

P. H. Wiebe, D. Chu, S. Kaartvedt, A. Hundt, W. Melle, E. Ona, and P. Batta-Lona, "The acoustic properties of *Salpa thompsoni*," ICES J. Mar. Sci. 67, 583–593 (2010) [doi: 10.1093/icesjms/fsp263].

Table I. Cetacean tissue properties of acoustic significance.

Species / Name Nomenclature: Klinowska (1991)	Tissue Type					Property Investigated					Approach Methods / To understand CT = computed tomography GLC = gas-liquid chromatography MRI = magnetic resonance imaging TLC = thin layer chromatography	Source	
	Nasal tissues	Phonic fat bodies	Auditory fat bodies	Blubber; musele	Bony tissues	Anatomy	Sound speed	Mass density	Pressure, temperature dependees	Biochemisty			
<i>Phocoena phocoena</i> / harbour porpoise; <i>Balaenaptera musculus</i> / blue whale; <i>Balaenoptera physalus</i> / fin whale				x		x						Morphology / Thermal properties; role of blubber	Parry (1949)
<i>Physeter macrcephalus</i> / sperm whale		x						x	x			Density analysis / Role of spermaceti organ in buoyancy	Clarke (1970)
<i>Physeter macrcephalus</i> / sperm whale		x									x	TLC; GLC; lipid & fatty acid analysis / Lipid structure of spermaceti organ	Morris (1973)
<i>Globicephala melas</i> / long-finned pilot whale		x				x						Dissection; lipid analysis; TLC; GLC / Role of melon lipids in echolocation	Wedmid et al. (1973)
<i>Tursiops truncatus</i> / bottlenose dolphin		x					x					Acoustic time-of-flight measurements / Sound transmission in head	Norris & Harvey (1974)
Odontocetes		x										Lipid extraction; TLC; infared spectroscopy / Role of melon fats in echolocation	Litchfield & Greenberg (1974)
Odontocetes	x	x	x	x								TLC; lipid & fatty acid analysis; Wijs method / Echolocation mechanisms	Litchfield et al. (1975)
<i>Physeter macrcephalus</i> / sperm whale		x				x						Dissection; TLC; GLC / Spermaceti organ function	Morris (1975)
Porpoises & small whales	x	x	x				x	x	x			Density; TLC; lipid analysis; ultrasound / Acoustic lens for echolocation	Varanasi et al. (1975)
<i>Balaenaptera borealis</i> / sei whale				x		x						Dissection; histology; lipid analysis / Sei whale blubber	Ackman et al. (1975)
<i>Glalicephala melas</i> / long-finned pilot whale		x					x		x			Ultrasound / Role of melon in echolocation.	Blomberg & Jensen (1976)
<i>Glalicephala melas</i> / long-finned pilot whale		x					x					TLC; radioisotopes; ultrasound / Sound velocities in melon.	Blomberg & Lindholm (1976)
<i>Kogia breviceps</i> / pygmy sperm whale		x				x						Compositional topography; biochemistry; GLC; TLC / Echolocation	Karol et al. (1978)

Table I, continued. Cetacean tissue properties of acoustic significance.

Species / Name Nomenclature: Klinowska (1991)	Tissue Type					Property Investigated					Approach	Source
	Nasal tissues	Phonic fat bodies	Auditory fat bodies	Blubber; muscle	Bony tissues	Anatomy	Sound speed	Mass density	Pressure, temperature dependences	Biochemistry	Methods / To understand CT = computed tomography GLC = gas-liquid chromatography MRI = magnetic resonance imaging TLC = thin layer chromatography	
<i>Physeter macrocephalus</i> / sperm whale	x	x				x		x	x		Dissection; morphometry / Structure & function of spermaceti organ	Clarke (1978a)
<i>Physeter macrocephalus</i> / sperm whale		x						x	x	x	Head oil pressure & temperature measurements / Buoyancy function.	Clarke (1978b)
<i>Physeter macrocephalus</i> / sperm whale		x						x	x		Modeling / Buoyancy control.	Clarke (1978c)
<i>Physeter macrocephalus</i> / sperm whale			x	x		x				x	Dissection; biochemistry of lipids & viscera / Functions of fat distribution	Lockyer (1991)
<i>Kogia simus</i> / dwarf sperm whale.		x					x		x		Dissection; velocimetry / Melon function	Goold & Clarke (2000)
<i>Kogia breviceps</i> / pygmy sperm whale; <i>Kogia simus</i> / dwarf sperm whale	x	x				x	x		x		Dissection; thermal analysis / Sound production & conduction; buoyancy control	Clarke (2003)
Odontocetes		x		x		x				x	Dissection; fatty acid analysis; GLC / Roles of isovaleric acid	Koopman et al. (2003, 2006)
<i>Ziphius cavirostris</i> / Cuvier's beaked whale	x	x	x	x	x	x	x	x	x		Dissection; CT scans; velocimetry / Physical property values determined for modeling	Soldevilla et al. (2005)
<i>Ziphius cavirostris</i> / Cuvier's beaked whale	x	x	x	x	x	x	x	x			CT scans; 3D reconstruction; velocimetry; finite element modeling / Physical effect of sound	Krysl et al. (2006)
<i>Tursiops truncatus</i> / bottlenose dolphin		x	x	x	x	x	x	x	x		CT scans; X-ray; velocimetry / Postmortem changes; tissue structure; viscoelastic properties	McKenna et al. (2007)
<i>Ziphius cavirostris</i> / Cuvier's beaked whale	x	x	x		x	x		x			Dissection; CT scans / Sound transmission & reception	Cranford et al. (2008b)
<i>Phocoena phocoena</i> / harbour porpoise	x	x				x					Dissection; CT scans; MRI; Amira / Sound generation; echolocation	Huggenberger et al. (2009)

Table II. Tourmaline gauge placement in the common dolphin specimen. The Cable ID denotes the designation of the gauge signal in the PCB multi-channel signal conditioner model 481.

Gauge No.	Cable ID	Location	Depth (mm)
186	M	Nares	120
112	H	Left lung	130
187	N	Right lung	110
115	I	Thorax	120
90	K	Melon	40
188	O	Right ear	-
171	J	Abdomen	-
05	F	Epaxial muscle	25

Table III. Source levels of the ITC-1032 spherical transducer in units of decibels re 1 μ Pa at 1 m.

Source Location	Frequency (kHz)		
	5	7	10
1 Front	158.6 \pm 0.3	164.0 \pm 0.2	169.6 \pm 0.1
2 Right side	157.5 \pm 0.3	162.1 \pm 0.1	172.1 \pm 0.1
3 Left side	155.3 \pm 0.2	164.9 \pm 0.1	168.9 \pm 0.1

Table IV. Acoustic source locations external to the common dolphin specimen.

Location	Description
1	10 cm in front of rostrum
2	75 cm aft of tip of rostrum, 67 cm to right of specimen centerline as viewed from above
3	120 cm aft of tip of rostrum, 95 cm to left of specimen centerline as viewed from above, 35 cm above centerline

Table V. Statistical characteristics of the arrival time, Part A, and amplitude, Part B, of the signals in five tourmaline pressure gauges used as receiving sensors. These are based on the arrival time and amplitude of the matched-filter peak for the direct-path transmission in the external receiving sensor, designated Cable B, and sonar-induced pressure fields in the receiving sensors implanted in the epaxial muscle, Cable F, melon, Cable K, nares, Cable M, and right lung, Cable N. When the acoustic source was on the left side of the specimen and transmitted at 5 kHz, only four transmit signals were recorded on Cable Z, hence only four received signals in the implanted sensors were analyzed. In all other cases, the entire set of 20 transmit and received signals were analyzed.

A. Arrival time in milliseconds				
Source location	Receiver location	5 kHz	7 kHz	10 kHz
Front	B: External	0.34 ± 0.01	0.37 ± 0.01	0.37 ± 0.00
	F: Epaxial muscle	1.16 ± 0.24	2.79 ± 0.09	2.06 ± 1.76
	K: Melon	0.23 ± 0.02	0.25 ± 0.01	0.33 ± 0.00
	M: Nares	–	0.42 ± 0.09	0.62 ± 0.04
	N: Right lung	–	–	–
Right side	B: External	0.26 ± 0.01	0.25 ± 0.00	0.31 ± 0.00
	F: Epaxial muscle	0.58 ± 0.02	0.49 ± 0.01	0.57 ± 0.00
	K: Melon	0.80 ± 0.05	0.59 ± 0.03	0.67 ± 0.00
	M: Nares	0.60 ± 0.25	0.73 ± 0.05	0.37 ± 0.03
	N: Right lung	–	0.84 ± 0.15	0.75 ± 0.04
Left side	B: External	0.28 ± 0.01	0.37 ± 0.00	0.35 ± 0.00
	F: Epaxial muscle	0.86 ± 0.10	0.83 ± 0.04	0.80 ± 0.02
	K: Melon	0.78 ± 0.09	1.08 ± 0.03	0.94 ± 0.01
	M: Nares	–	–	1.04 ± 0.19
	N: Right lung	–	–	–
B. Signal magnitude in decibels				
Source location	Receiver location	5 kHz	7 kHz	10 kHz
Front	B: External	6.3 ± 0.3	5.6 ± 0.1	5.6 ± 0.1
	F: Epaxial muscle	-20.3 ± 1.0	-20.9 ± 0.9	-25.7 ± 0.8
	K: Melon	3.3 ± 0.3	3.9 ± 0.2	8.2 ± 0.1
	M: Nares	–	-20.1 ± 0.7	-20.3 ± 0.5
	N: Right lung	–	–	–
Right side	B: External	8.6 ± 0.3	8.9 ± 0.1	7.2 ± 0.1
	F: Epaxial muscle	-1.1 ± 0.4	-5.8 ± 0.2	-3.8 ± 0.1
	K: Melon	-3.2 ± 0.3	-7.3 ± 0.3	-4.9 ± 0.2
	M: Nares	-15.5 ± 0.8	-18.0 ± 0.8	-20.4 ± 0.5
	N: Right lung	–	-20.5 ± 1.0	-21.7 ± 0.4
Left side	B: External	8.0 ± 0.3	5.6 ± 0.1	6.1 ± 0.1
	F: Epaxial muscle	-13.6 ± 0.6	-14.3 ± 0.3	-13.3 ± 0.2
	K: Melon	-12.0 ± 1.2	-10.5 ± 0.3	-7.6 ± 0.2
	M: Nares	–	–	-28.5 ± 1.6
	N: Right lung	–	–	–

Table VI. Internal field values of pressure and particle displacement due to *point-source ensonification* of a fluid sphere immersed in water for each of two values of internal absorption: (a) $\alpha_1\lambda_1=0$ dB, and (b) $\alpha_1\lambda_1=10$ dB, where λ_1 is the internal wavelength. The sphere diameter $2a$ is 50 mm, mass density 1900 kg/m^3 , and sound speed 857 m/s. The water mass density is 1000 kg/m^3 and sound speed 1500 m/s. The point source is located 75 mm from the sphere center. Its source strength, q_0 in Eq. (1a), is 1 Pa m and its harmonic frequency is 100 kHz. The field point is described by its distance r from the sphere center and polar angle θ , which is the angle between the vector to the field point and longitudinal axis of the sphere. In the implied coordinate system, the source is located at $r_0=75$ mm and $\theta=180$ deg.

(a) $\alpha_1/\lambda_1 = 0$ dB/m										
r/a	θ (deg)	p_{int} (Pa)			u_r (pm)			u_θ (pm)		
		Real	Imag	Mag	Real	Imag	Mag	Real	Imag	Mag
-1.0	180	-12.2831	17.4343	21.3267	6.8180	7.4401	10.0916	0	0	0
-0.5	180	17.4377	-24.7762	30.2974	-13.3784	-6.8501	15.0301	0	0	0
0.0	-	1.1625	25.2769	25.3036	-22.8015	0.3063	22.8036	0	0	0
0.5	0	3.5059	-27.7566	27.9771	22.7649	-15.4230	27.4975	0	0	0
1.0	0	92.4330	84.0886	124.9590	-59.6620	20.0940	62.9549	0	0	0
0.5	30	-35.6583	-1.7023	35.6989	-5.8754	-23.3146	24.0435	1.4424	13.1947	13.2733
0.5	60	16.4382	-14.0547	21.6275	2.8506	6.7643	7.3405	-21.6775	-20.3666	29.7441
0.5	90	14.9343	19.0374	24.1962	2.0098	-1.9264	2.7840	13.2588	-11.8924	17.8108
0.5	120	-21.0330	5.6706	21.7840	3.8198	11.9976	12.5910	2.5568	16.8144	17.0077
0.5	150	21.5088	-3.7667	21.8361	-3.2086	-19.0306	19.2991	-5.4500	-8.8940	10.4310

(b) $\alpha_1/\lambda_1 = 10$ dB/m										
r/a	θ (deg)	p_{int} (Pa)			u_r (pm)			u_θ (pm)		
		Real	Imag	Mag	Real	Imag	Mag	Real	Imag	Mag
-1.0	180	-9.1557	18.4622	20.6077	16.5499	12.1381	20.5239	0	0	0
-0.5	180	1.0245	-4.0501	4.1777	-3.8124	-1.6951	4.1723	0	0	0
0.0	-	-0.0625	0.8516	0.8539	-0.8321	-0.2065	0.8573	0	0	0
0.5	0	-0.0861	-0.3580	0.3682	0.1392	-0.1555	0.2087	0	0	0
1.0	0	-0.2023	1.1073	1.1256	0.3110	0.3398	0.4606	0	0	0
0.5	30	-0.2370	-0.1888	0.3030	0.1210	-0.3134	0.3360	-0.2170	0.0531	0.2234
0.5	60	0.8397	-0.4586	0.9568	0.2491	0.1052	0.2704	-0.3270	-0.8924	0.9504
0.5	90	0.9890	1.3942	1.7094	0.4617	-0.0396	0.4634	1.4422	-0.8068	1.6525
0.5	120	-2.6234	0.6554	2.7040	0.0083	1.6722	1.6722	0.2995	2.1047	2.1259
0.5	150	3.6525	-0.7000	3.7190	-0.0197	-3.3134	3.3134	-0.1461	-1.6761	1.6824

Table VII. Internal field values of pressure and particle displacement due to *plane-wave ensonification* of a fluid sphere immersed in water for each of two values of internal absorption: (a) $\alpha_1 \lambda_1 = 0$ dB, and (b) $\alpha_1 \lambda_1 = 10$ dB, where λ_1 is the internal wavelength. The sphere diameter $2a$ is 50 mm, mass density 1900 kg/m^3 , and sound speed 857 m/s. The water mass density is 1000 kg/m^3 and sound speed 1500 m/s. The plane wave propagates along the longitudinal axis of the sphere. Its amplitude, p_0 in Eq. (5a), is 1 Pa and its harmonic frequency is 100 kHz. The field point is described by its distance r from the sphere center and polar angle θ , which is the angle between the vector to the field point and longitudinal axis of the sphere. In the implied coordinate system, the source is located at infinity with $\theta = 180$ deg.

(a) $\alpha_1 / \lambda_1 = 0$ dB/m										
r/a	θ (deg)	p_{int} (Pa)			u_r (pm)			u_θ (pm)		
		Real	Imag	Mag	Real	Imag	Mag	Real	Imag	Mag
-1.0	180	-0.9584	2.6523	2.8202	1.5752	-0.0441	1.5759	0	0	0
-0.5	180	-0.1511	-2.0656	2.0711	-1.5746	-0.7560	1.7467	0	0	0
0.0	-	0.0872	1.8958	1.8978	-1.7077	0.0773	1.7094	0	0	0
0.5	0	0.2950	-3.0623	3.0765	3.0427	-0.6949	3.1210	0	0	0
1.0	0	6.2740	-5.1387	8.1098	1.7021	6.2059	6.4351	0	0	0
0.5	30	-2.2938	2.1729	3.1596	-1.1312	-0.9730	1.4921	1.4993	1.3596	2.0240
0.5	60	-0.4380	-1.4250	1.4908	0.1945	0.1891	0.2713	-1.7900	1.0743	2.0876
0.5	90	1.6826	-0.5235	1.7622	-0.0992	-0.5083	0.5179	-0.1970	-0.9603	0.9803
0.5	120	-0.7858	1.1184	1.3669	0.8486	0.4313	0.9519	0.9485	0.5828	1.1132
0.5	150	1.1298	-0.5197	1.2436	-0.5815	-1.1602	1.2978	-0.0617	-0.2152	0.2238

(b) $\alpha_1 / \lambda_1 = 10$ dB/m										
r/a	θ (deg)	p_{int} (Pa)			u_r (pm)			u_θ (pm)		
		Real	Imag	Mag	Real	Imag	Mag	Real	Imag	Mag
-1.0	180	-0.4436	0.9290	1.0295	0.8426	0.5797	1.0228	0	0	0
-0.5	180	0.0570	-0.2399	0.2465	-0.2276	-0.0917	0.2454	0	0	0
0.0	-	-0.0047	0.0639	0.0640	-0.0628	-0.0135	0.0643	0	0	0
0.5	0	-0.0156	0.0172	0.0232	-0.0034	0.0307	0.0309	0	0	0
1.0	0	0.1822	-0.0517	0.1894	0.0008	-0.0997	0.0997	0	0	0
0.5	30	-0.0587	0.0159	0.0608	-0.0249	-0.0235	0.0342	-0.0005	0.0570	0.0570
0.5	60	-0.0309	-0.0998	0.1045	-0.0101	-0.0144	0.0176	-0.1025	0.0224	0.1049
0.5	90	0.1459	-0.0382	0.1508	0.0050	-0.0682	0.0684	-0.0248	-0.1322	0.1345
0.5	120	-0.1076	0.1660	0.1978	0.1038	0.1022	0.1456	0.1069	0.0799	0.1334
0.5	150	0.2119	-0.0977	0.2334	-0.0579	-0.2085	0.2164	-0.0308	-0.0793	0.0851

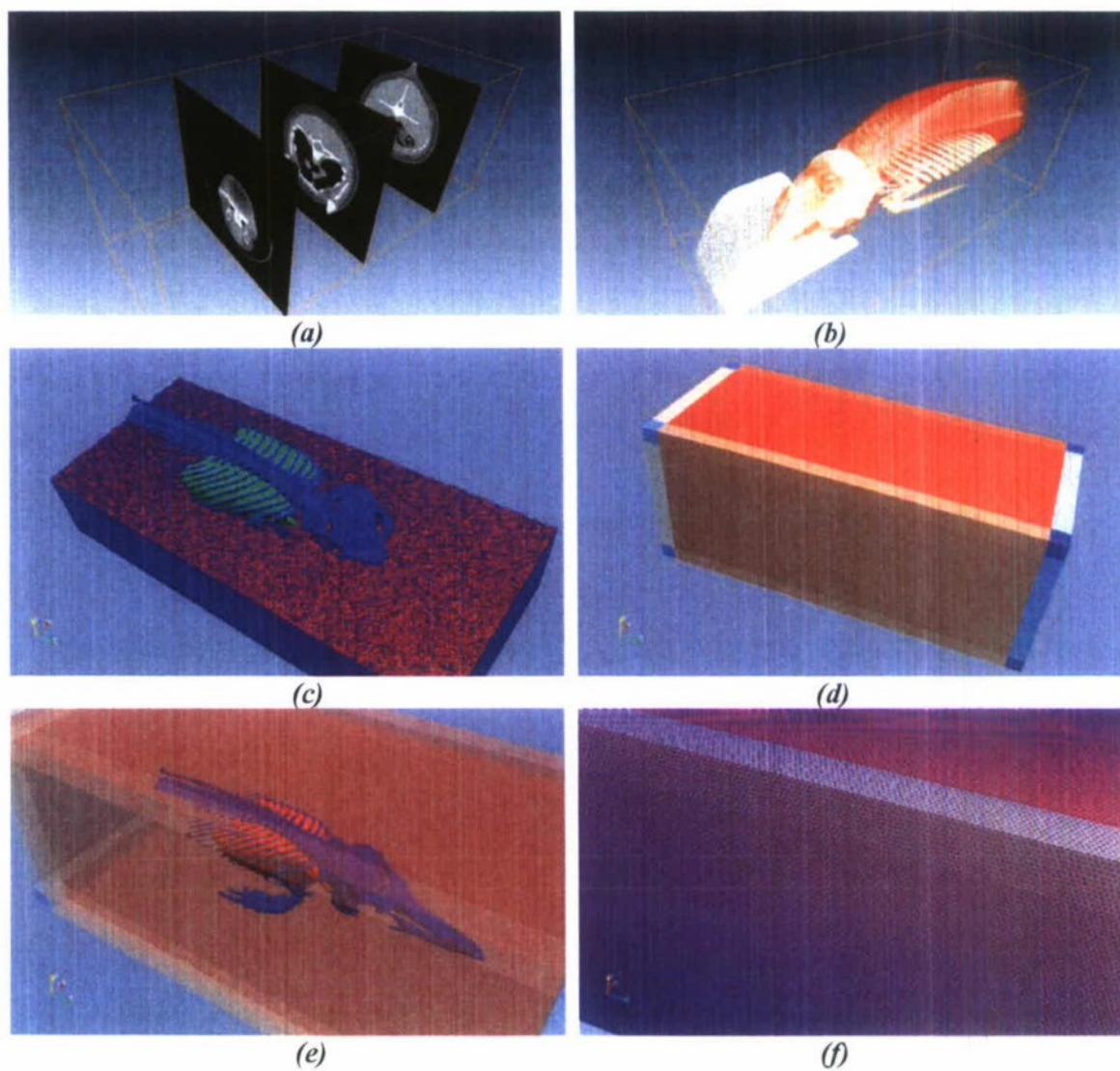
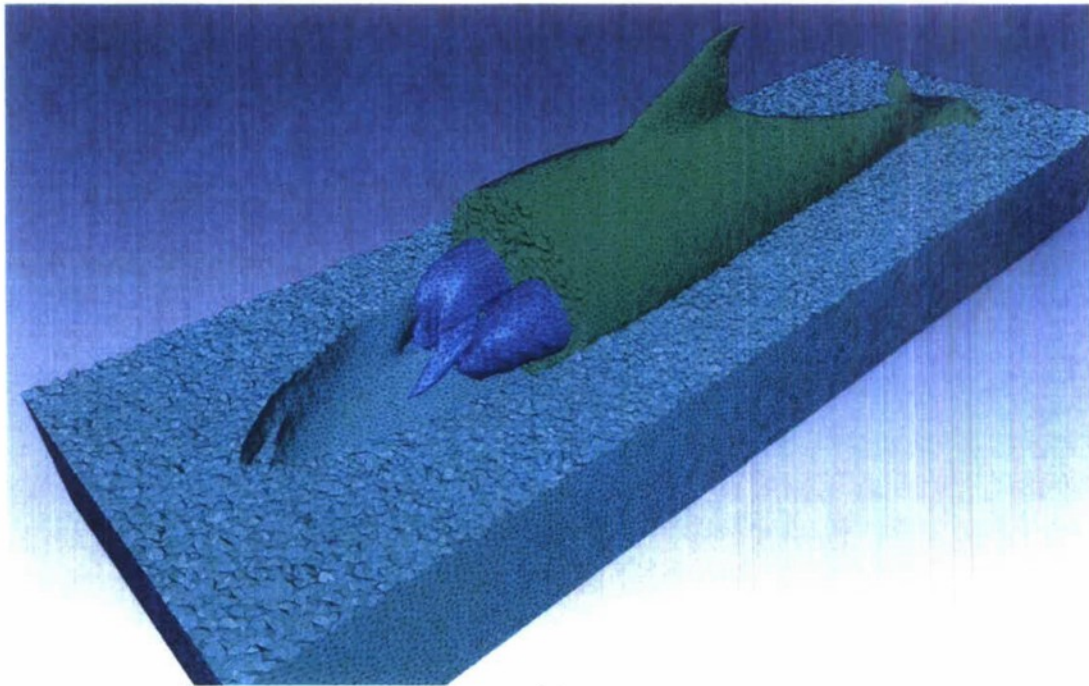
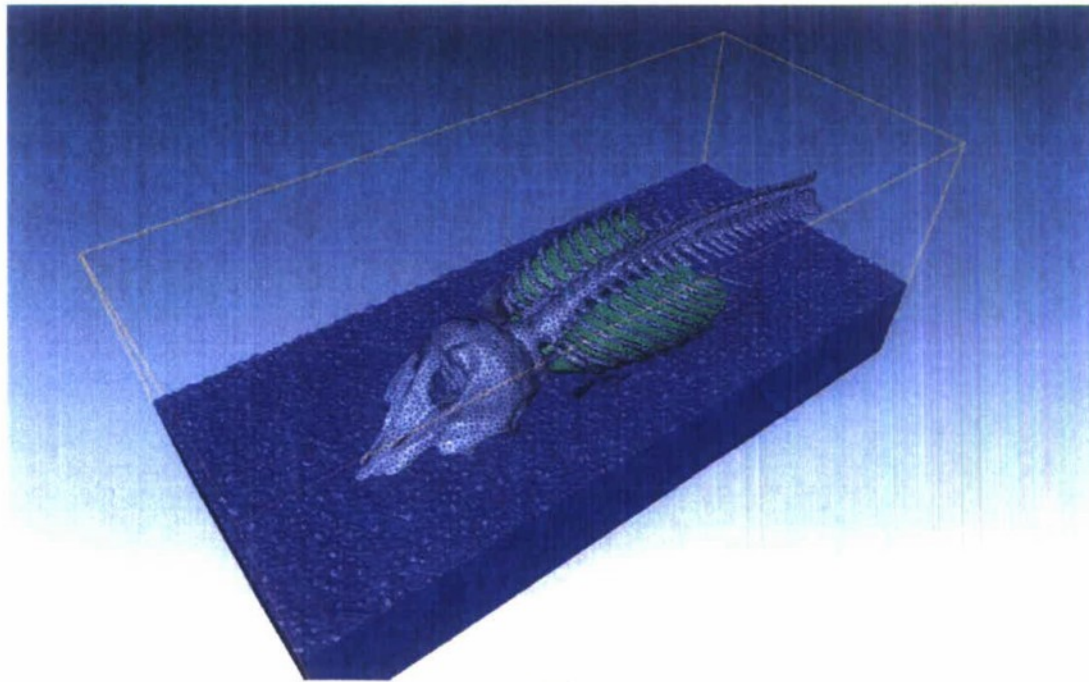


Fig. 1. Construction of the finite-element mesh for a 142-cm-long common dolphin. From CT images (a), surface reconstructions of tissues can be obtained (b). These surfaces are sub-sampled and triangulations of the interfaces are created. From these triangulations, a tetrahedral mesh is created (c), illustrated in greater detail in Figs. 2–4. An external mesh, which is necessary for acoustic computations, is constructed and joined with the previous mesh. An outline of this is shown in (d), with different perfectly matched layer blocks shown in color. The meshed dolphin within the computational volume is shown in (e). A detail of the triangulation in the surface of the external mesh is shown in (f).

Credit: G. Feijoo, D. Ketten.

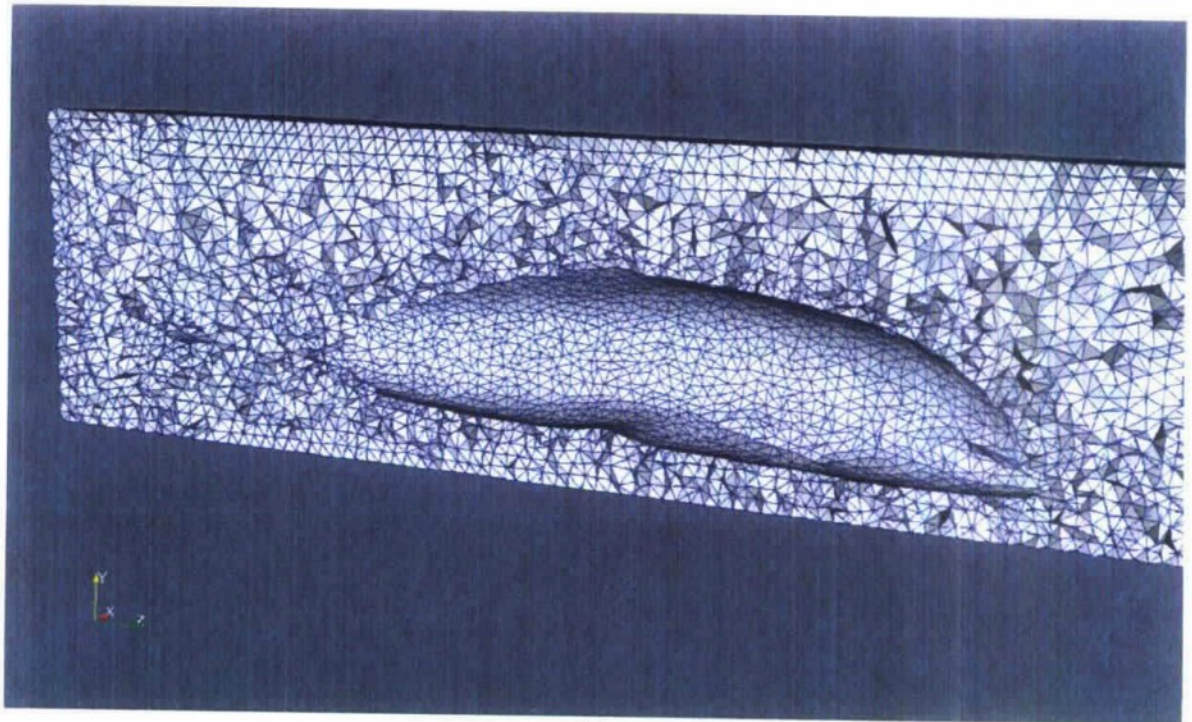


(a)

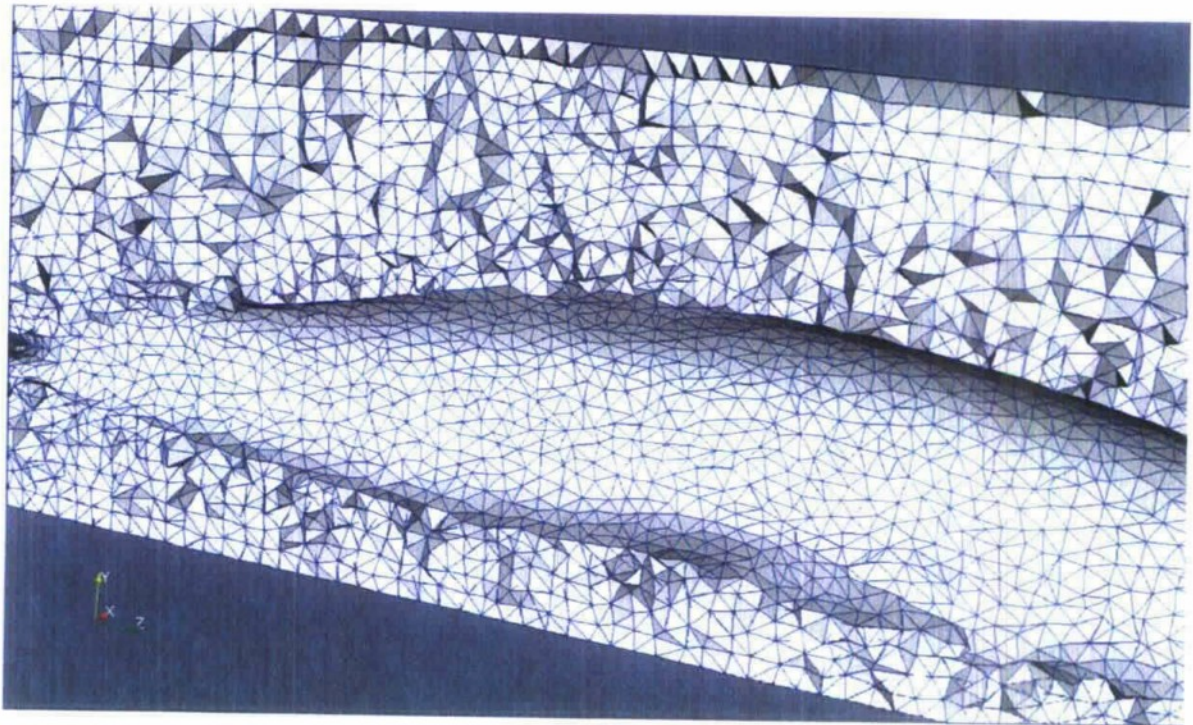


(b)

Fig. 2. Finite-element representation with tetraheda of a 142-cm-long common dolphin and external, computational volume, in two views. (a) The lungs are indicated in blue. (b) The skeleton is indicated in gray and the lungs, in green. Credit: G. Feijoo, D. Ketten.

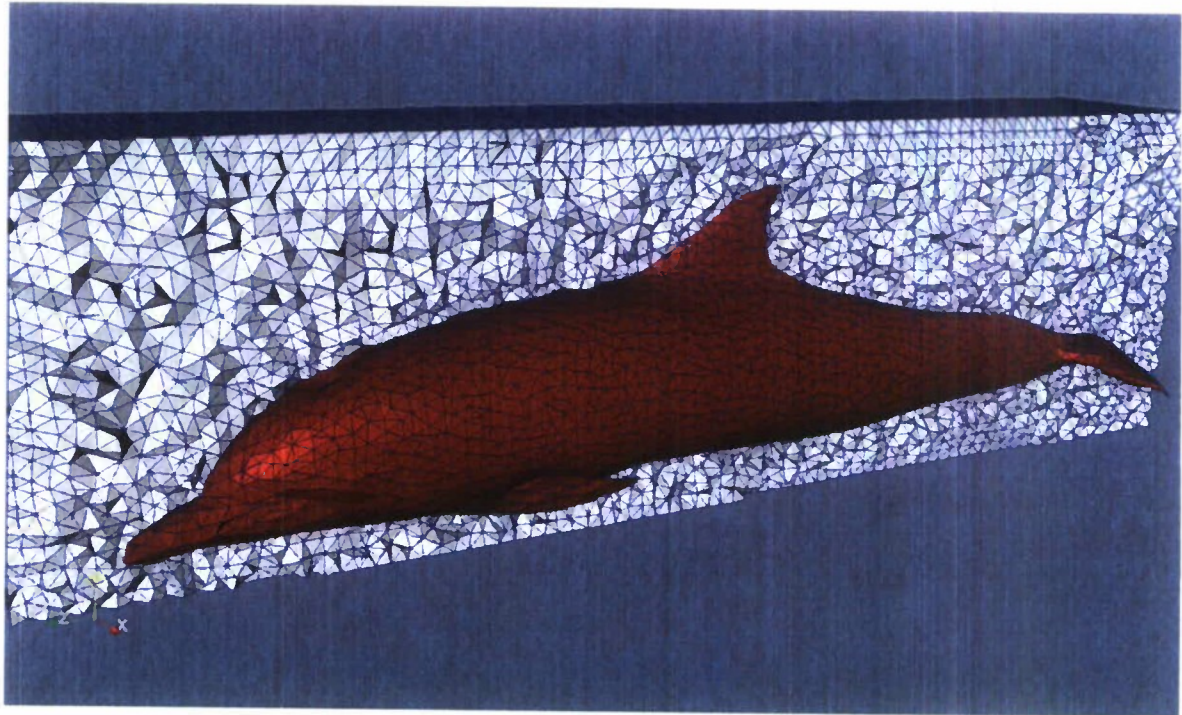


(a)

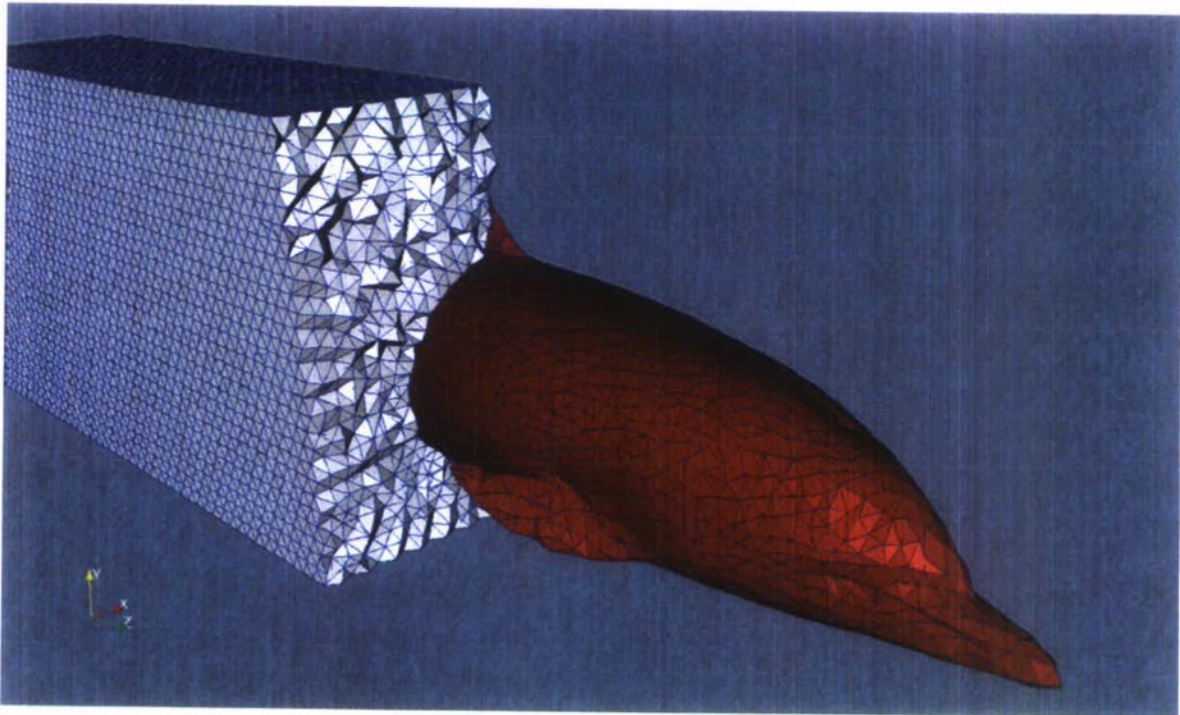


(b)

*Fig. 3. Details of tetrahedral meshing for the common dolphin specimen in Fig. 2.
Credit: G. Feijoo, D. Ketten.*

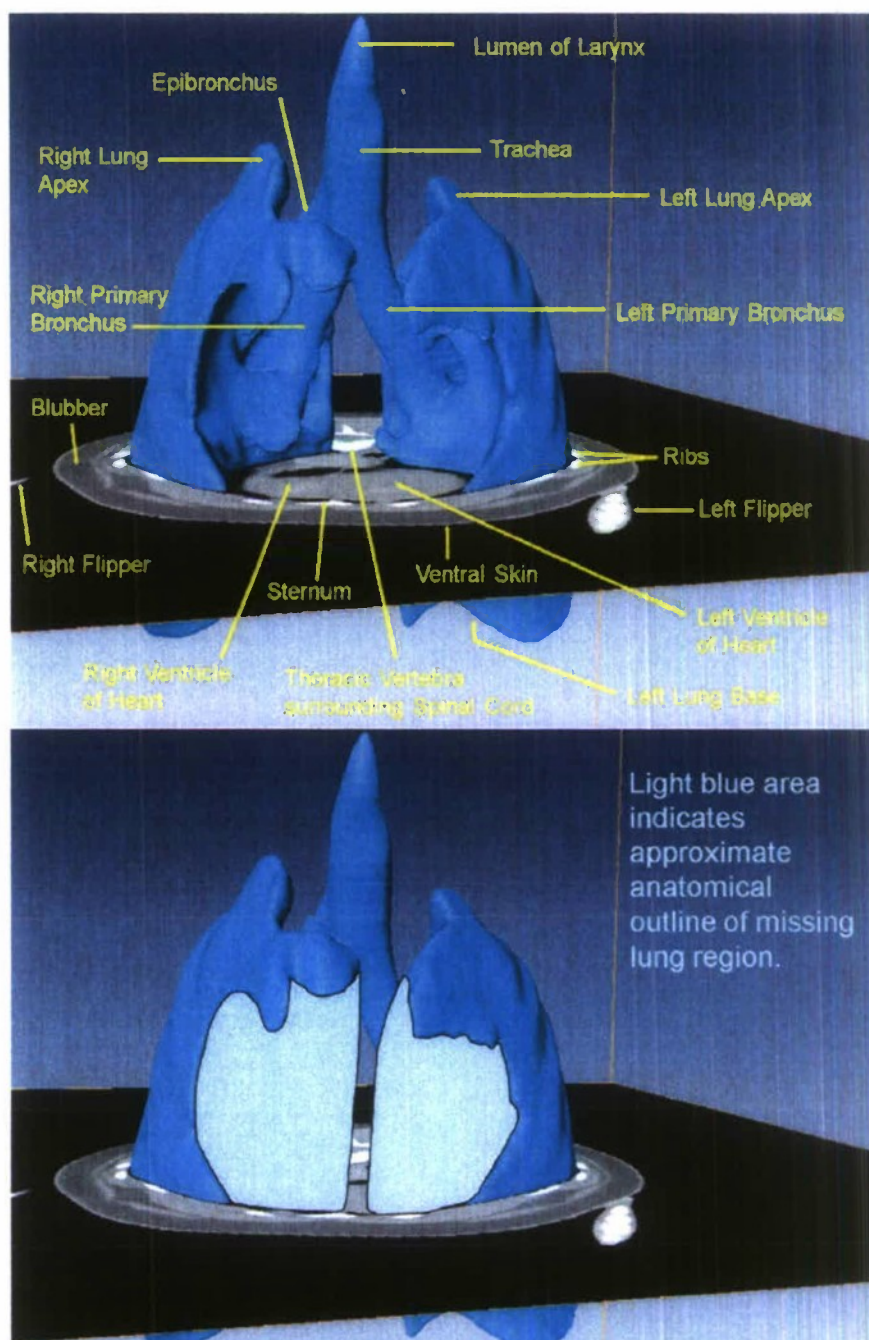


(a)



(b)

Fig. 4. Further details of tetrahedral meshing for the common dolphin specimen in Figs. 2 and 3. Credit: G. Feijoo, D. Ketten.



Higher CT scan resolution will provide better discrimination between thin layers of air filled lung and adjoining soft tissues.

Fig. 5. Three-dimensional surface rendering, based on CT scans visualized with Amira, of the lower respiratory tract in a 142-cm-long common dolphin specimen, with superimposed transverse CT section. Upper panel: lower respiratory tract and nearby tissues labeled. Lower panel: missing lung volumes indicated. Credit: J. Reidenberg.

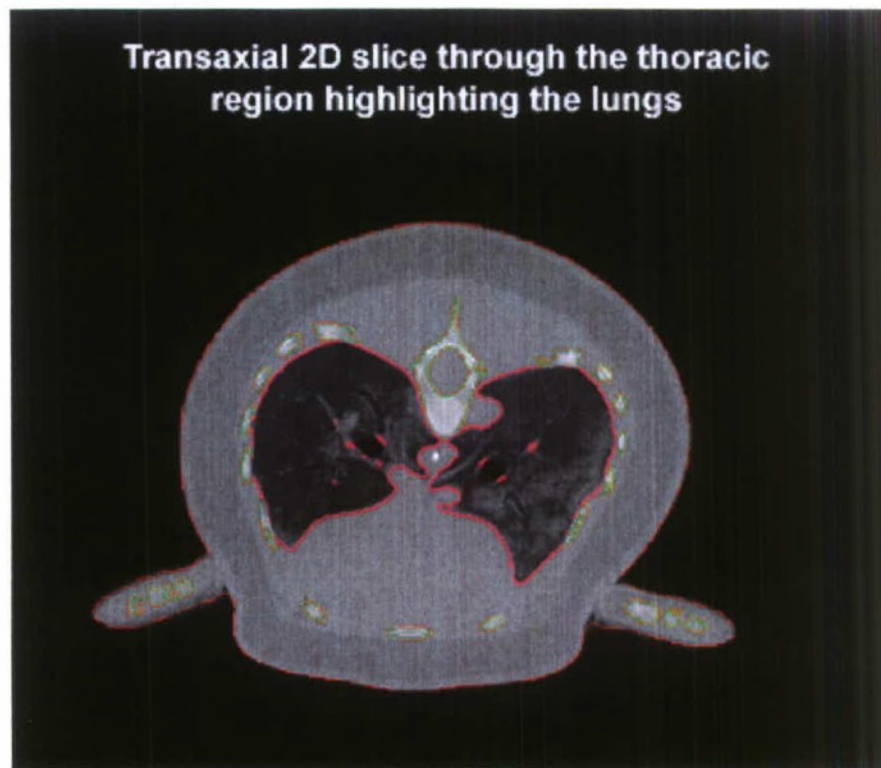
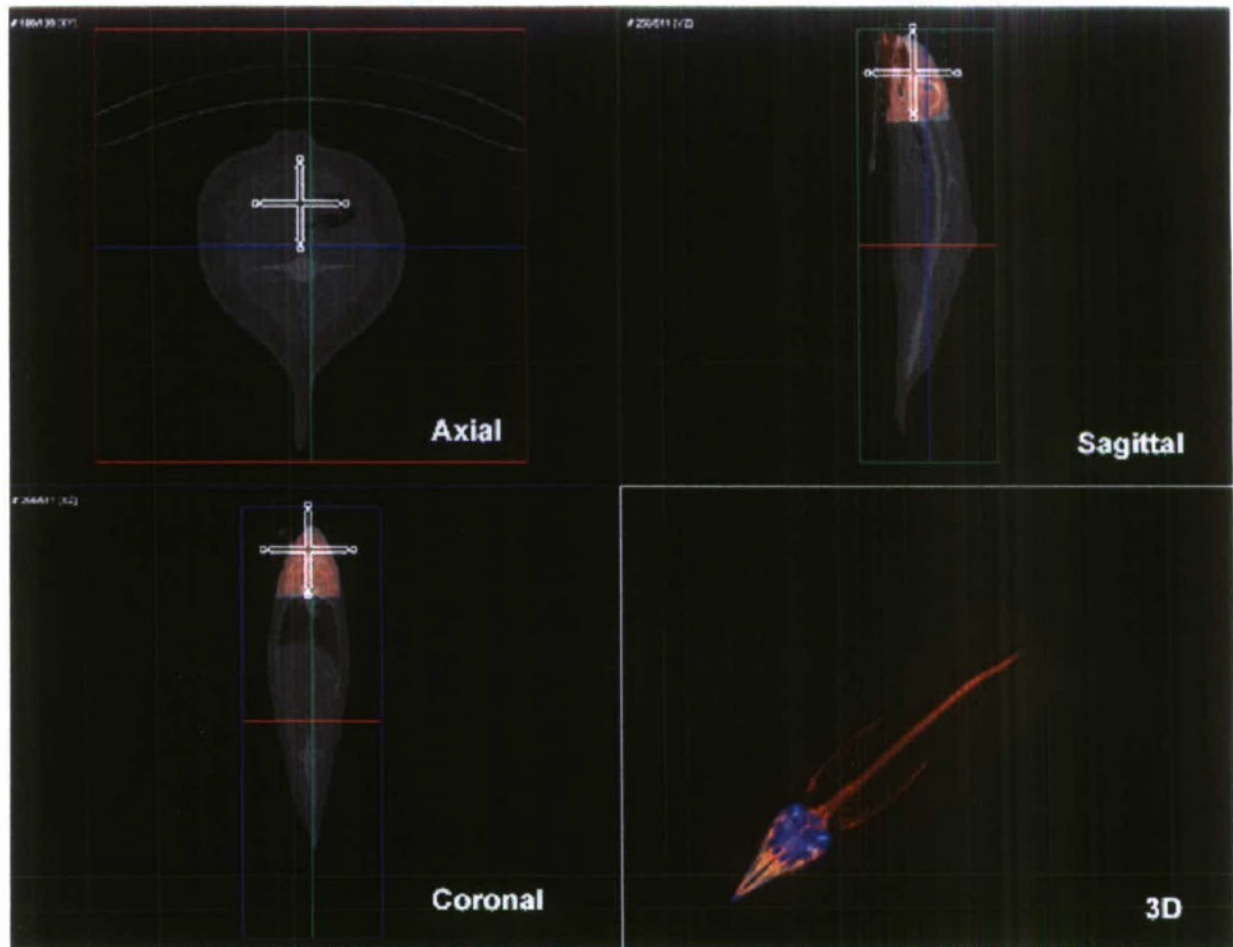


Fig. 6. Transaxial two-dimensional slice through the thoracic region of the synthetic model of a beaked whale, with lungs outlined in red, and skeleton, consisting of ribs, one vertebra, and bones in the pectoral flippers, outlined in green. Credit: D. Ketten, S. Cramer.



*Fig. 7. Axial, sagittal, and coronal views of the synthetic model of a beaked whale, together with a dorsal transparent view highlighting the skeleton and air passages.
Credit: D. Ketten, S. Cramer.*

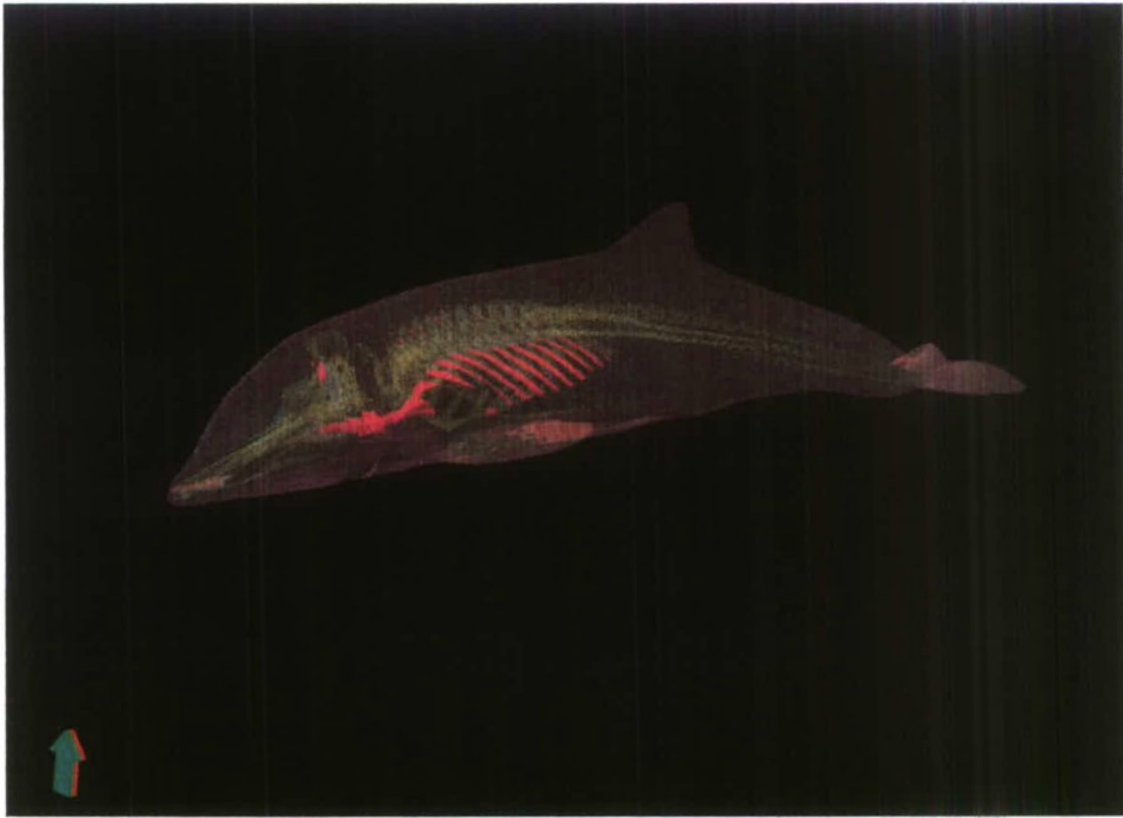
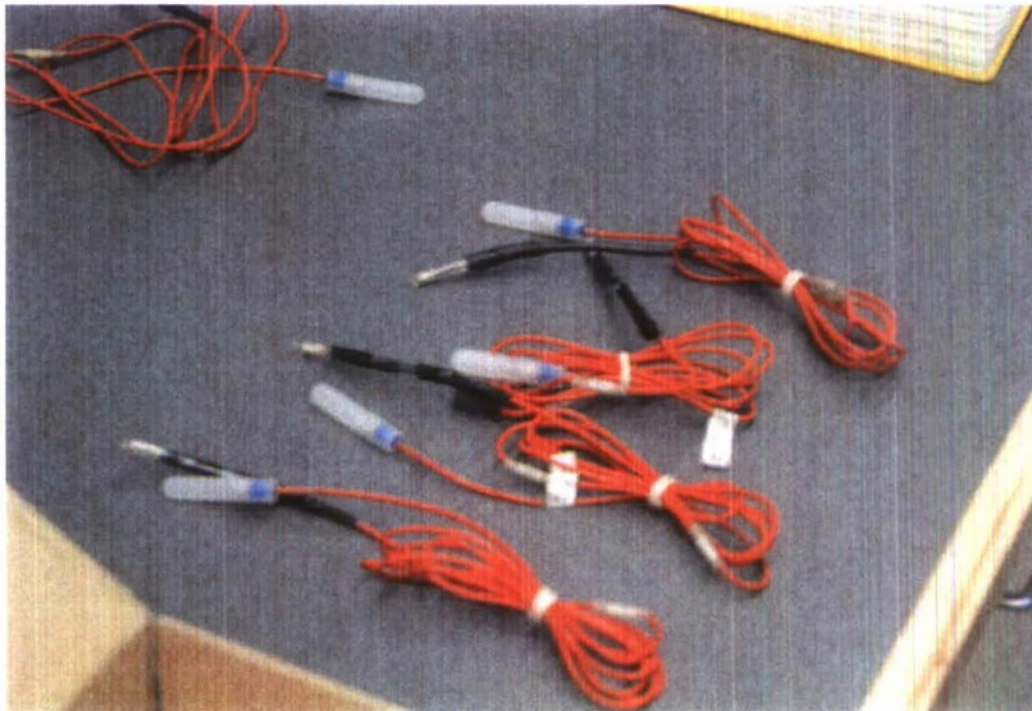


Fig. 8. Left lateral transparent view of the synthetic model of a beaked whale, highlighting the skeleton, air passages, and exterior surface. Credit: D. Ketten, S. Cramer.



(a)



(b)

Fig. 9. (a) The experimental subject, a 119-kg, 211-cm-long common dolphin specimen, following implantation of several tourmaline pressure sensors (b) at the WHOI CSI Facility. Credit: D. Ketten, S. Cramer, J. Aruda.



(a)



(b)

Fig. 10. The experimental subject during implantation of tourmaline pressure sensors at the WHOI CSI Facility, (a) with use of the CT scanner to confirm sensor placements, and (b) following completion of sensor placements. Credit: D. Ketten, S. Cramer, J. Aruda.

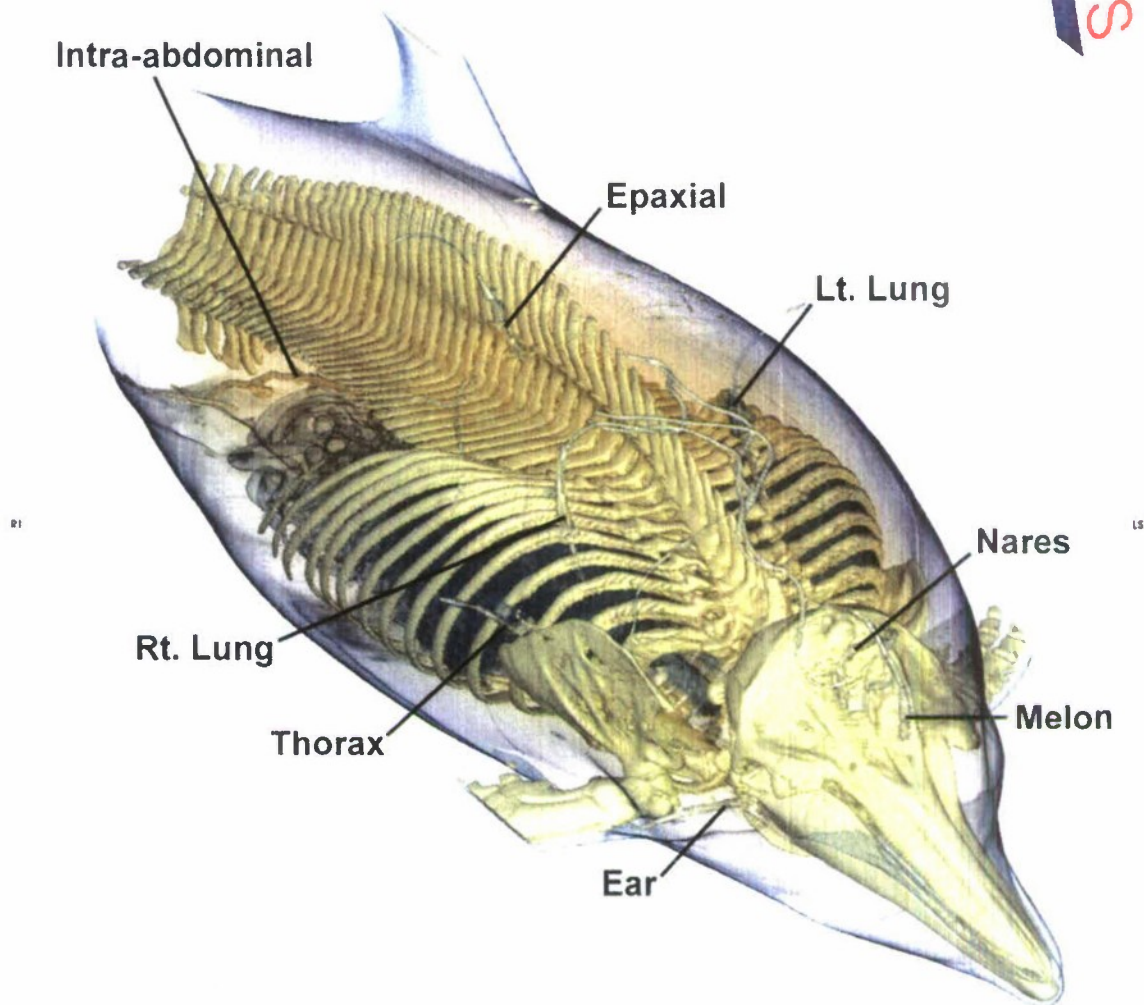


Fig. 11. Gauge placements in the common dolphin specimen according to a virtual ray tracing (VRT) three-dimensional image, which also includes the lungs, skeleton, and skin for reference. Credit: D. Ketten, S. Cramer, J. Aruda.

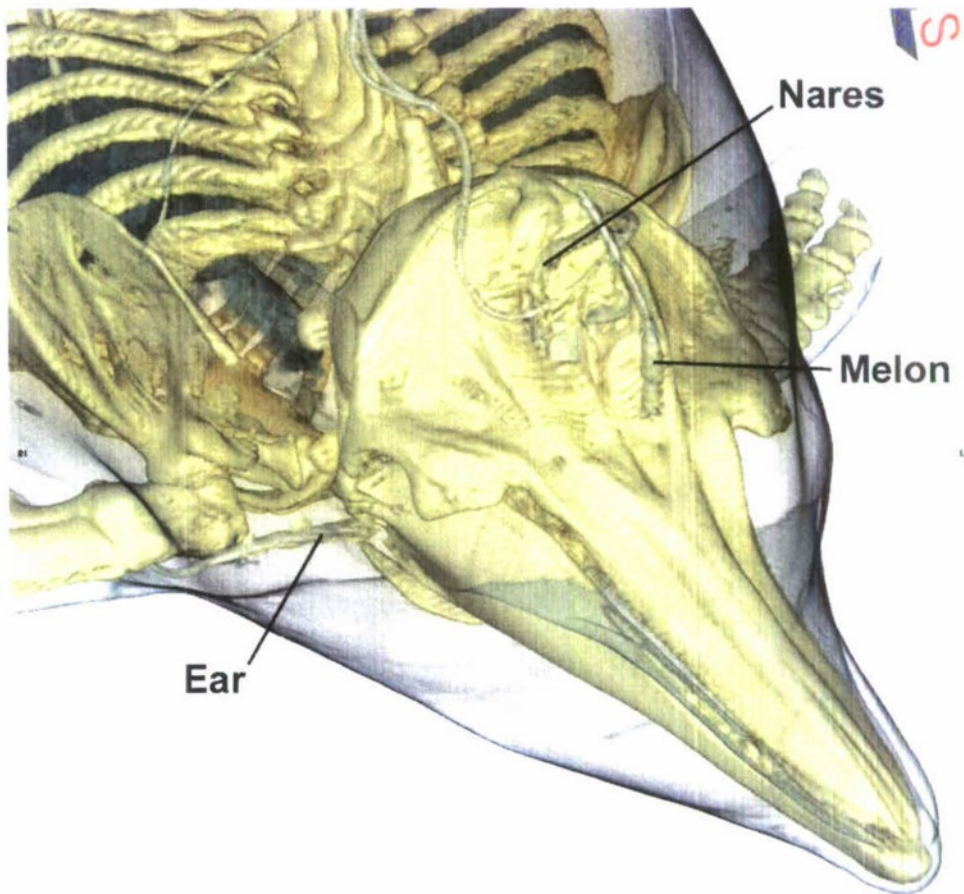


Fig. 12. Head gauge placements in the melon, nares, and ear of the common dolphin specimen whose virtual ray tracing (VRT) three-dimensional image is shown in Fig. 11, which also includes the lungs, skeleton, and skin for reference.

Credit: D. Ketten, S. Cramer, J. Arudu.



Fig. 13. The experimental subject, a 119-kg, 211-cm-long common dolphin specimen, following implantation of tourmaline sensors at the WHOI CSI Facility, suspended from a PVC-pipe frame at NSWC Carderock Division on 4 February 2009. Credit: D. Ketten, S. Cramer, K. Rye, W. H. Lewis, M. Hastings.

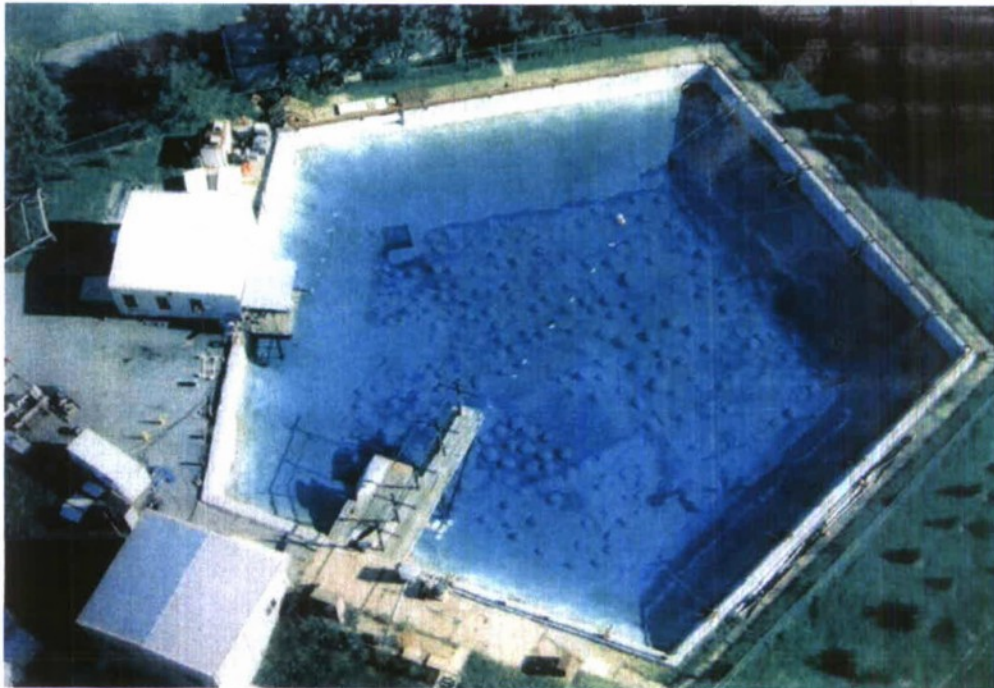


Fig. 14. Explosion Test Pond facility at NSWC Carderock Division: bird's-eye view.



Fig. 15. Specimen in its suspension frame being lowered into the pond by a crane. Credit: D. Ketten, S. Cramer, K. Rye, W. H. Lewis, M. Hastings.

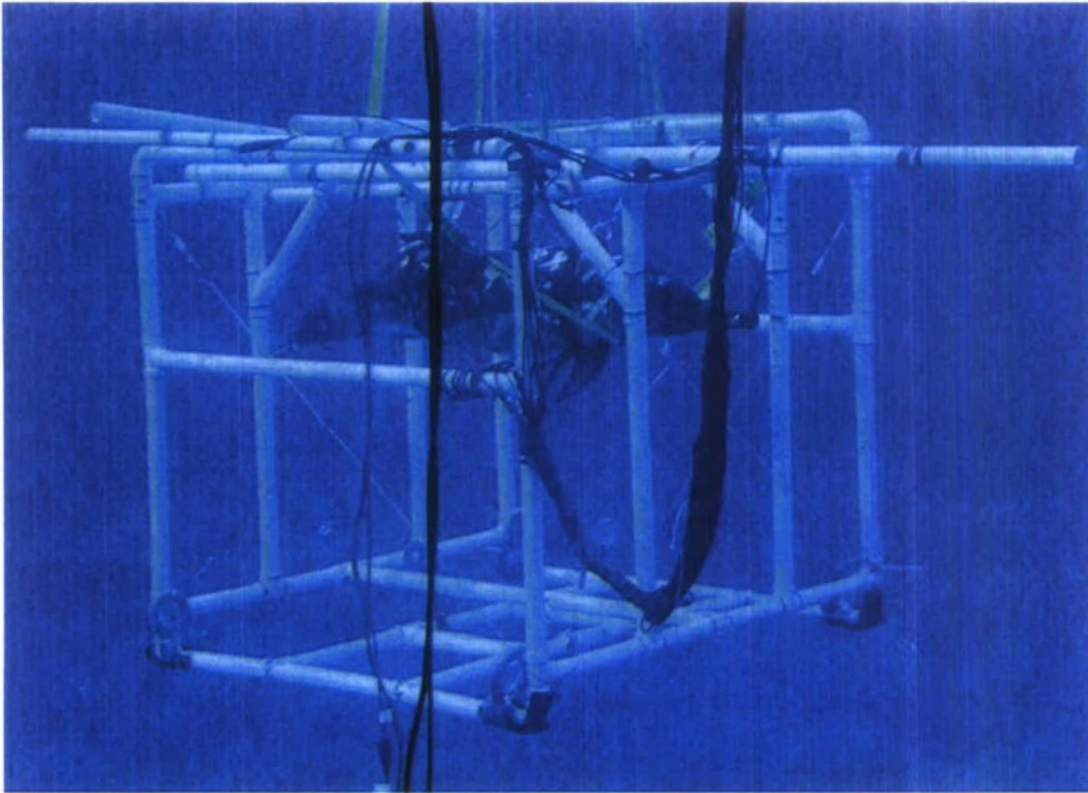


Fig. 16. The experimental subject, a 119-kg, 211-cm-long common dolphin specimen, following implantation of tourmaline sensors at the WHOI CSI Facility, suspended from a PVC-pipe frame at NSW Carderock Division on 4 February 2009, and immersed in the NSW Explosion Test Pond facility for acoustic measurement, lower frame.

Credit: D. Ketten, S. Cramer, K. Rye, W. H. Lewis, M. Hastings.

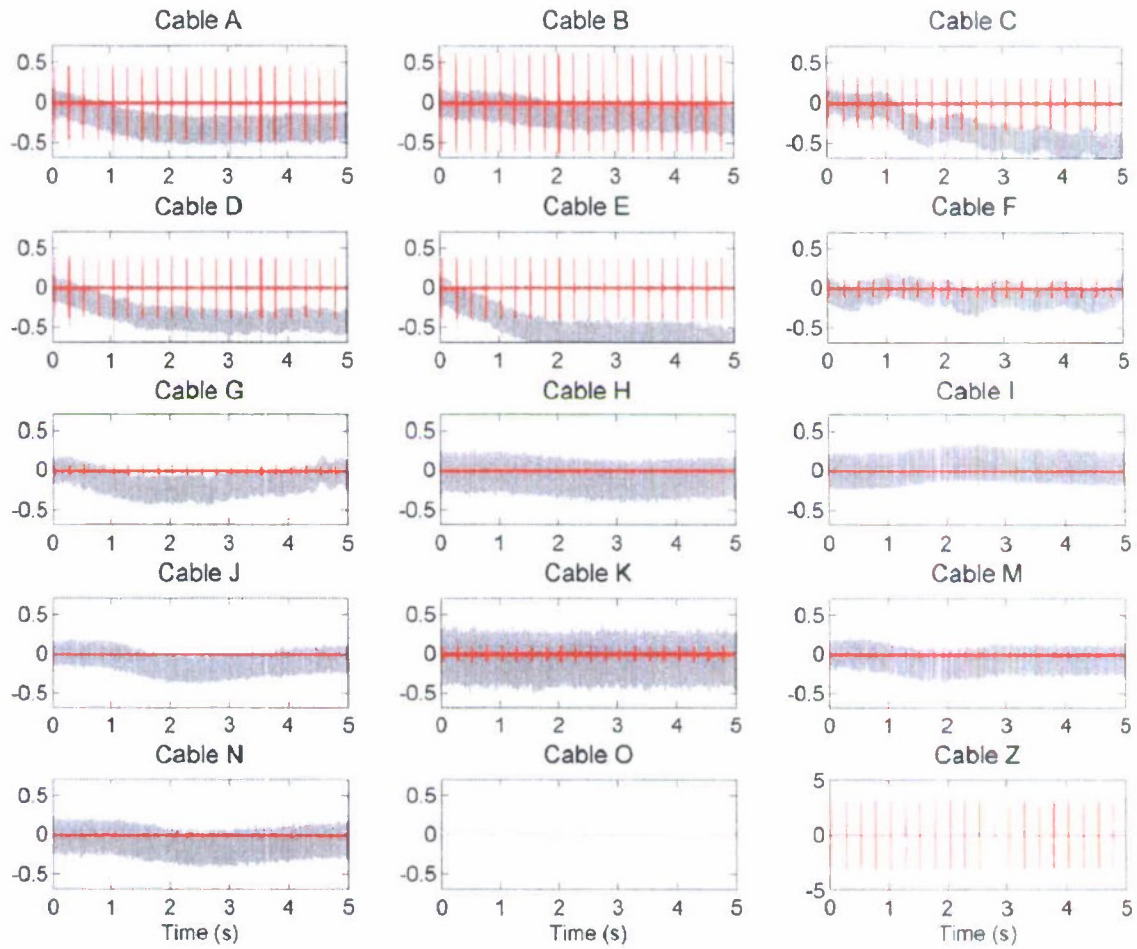


Fig. 17. Overview of acoustic data collected during the experiment with the common dolphin specimen at NSW Carderock Division on 4 February 2009 with the ITC-1032 spherical transducer on the right side of the specimen and transmit signal centered at 7 kHz. The total data collection time is 5 s; the pulse repetition frequency is 4 Hz. The total signal, including background noise, is shown in gray. The signal resulting from digital bandpass filtering with bandwidth equal to one-third of the center frequency is shown in red. Cables A, B, C, D, E, and G are connected to external sensors. Implanted sensors are connected to Cable F for the epaxial muscle near the dorsal fin, Cable H for the left lung, Cable I for the thorax, Cable J for the abdomen, Cable K for the melon, Cable M for the nares, Cable N for the right lung, and Cable O for the right ear. Credit: Y.-T. Lin, M. Hastings, K. Rye, K. Foote.

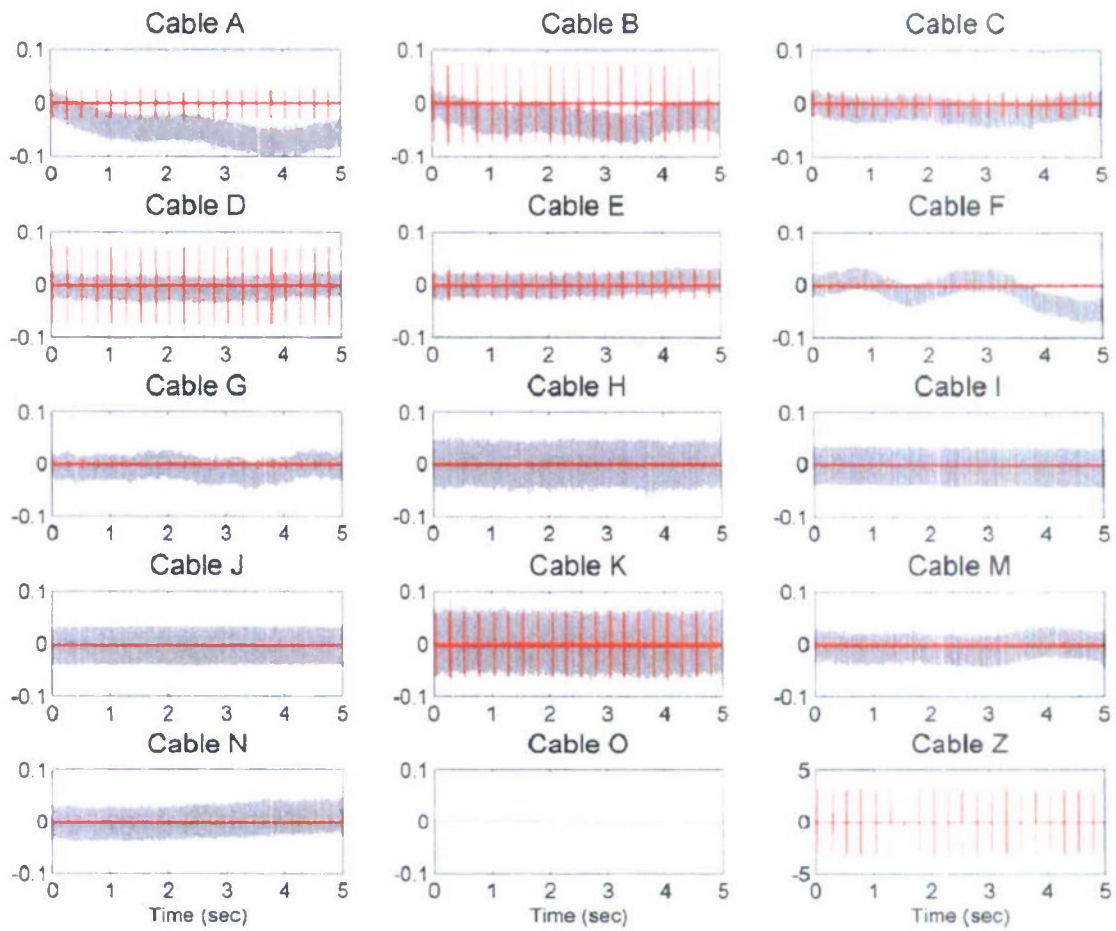
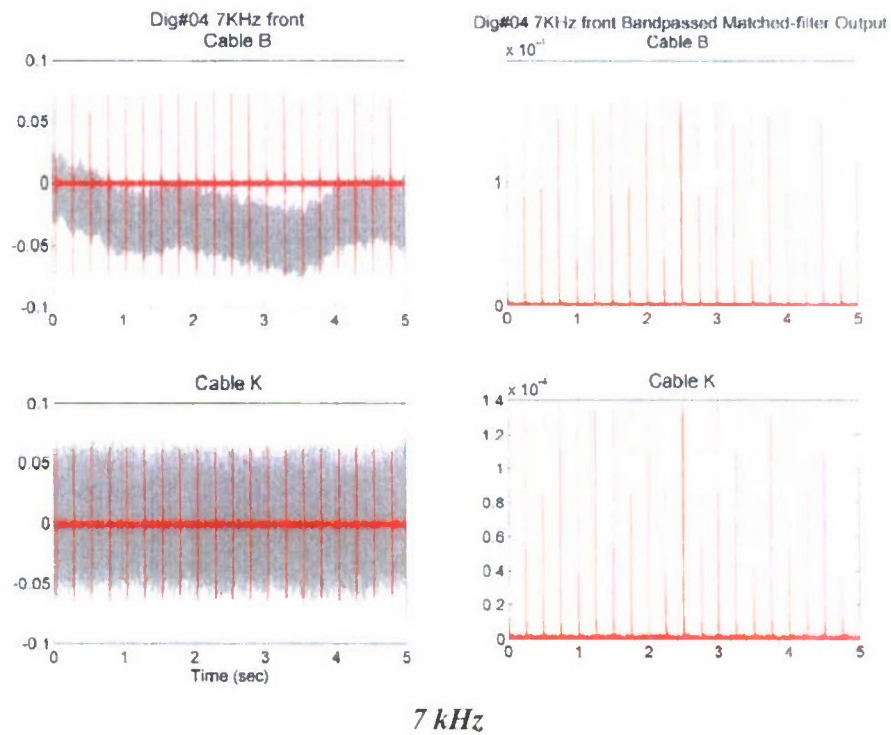
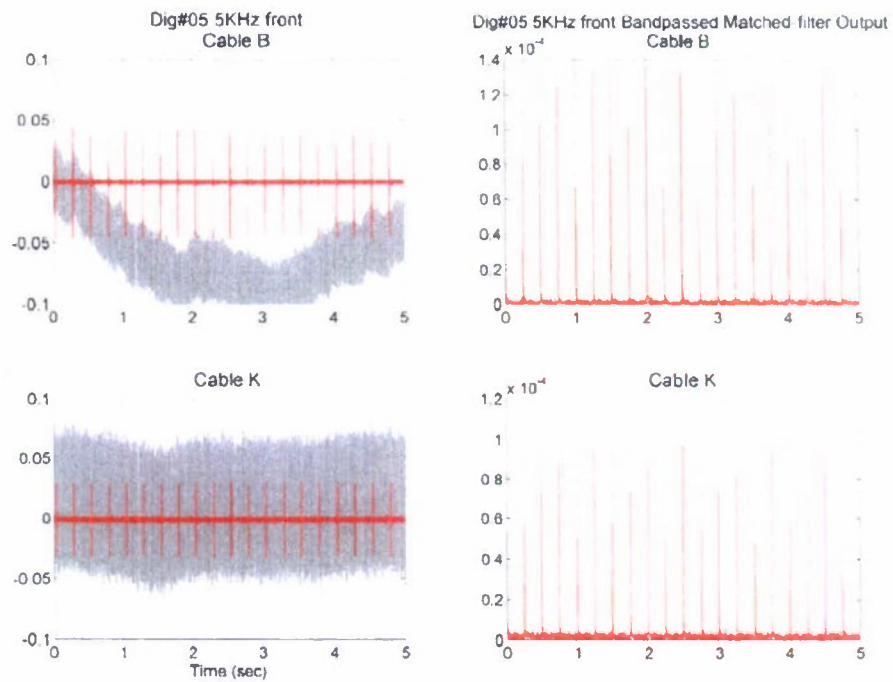


Fig. 18. Overview of acoustic data, as in Fig. 17, but with the spherical transducer in front of the specimen, again with the transmit signal centered at 7 kHz.

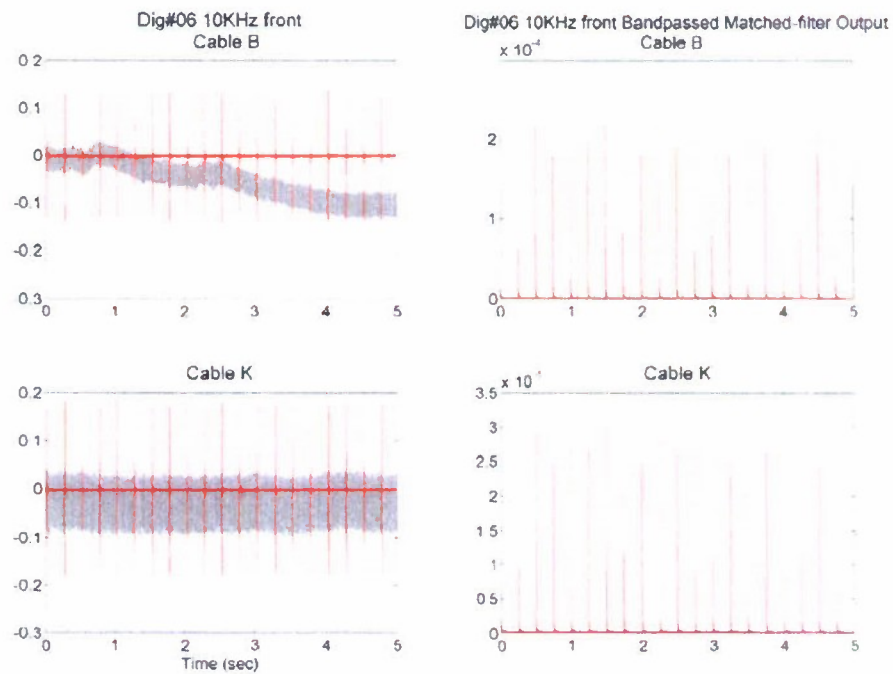


7 kHz

Fig. 19. Acoustic data from Fig. 18 together with results of band-pass and matched-filtering for external sensor B in the line of sight of the spherical transducer in front of the specimen and internal sensor K implanted in the melon, with the transmit signal centered at 7 kHz.



(a) 5 kHz



(b) 10 kHz

Fig. 20. Details of acoustic data for external sensor B in the line of sight of the spherical transducer in front of the specimen and internal sensor K implanted in the melon, with the transmit signal centered at (a) 5 kHz and (b) 10 kHz.

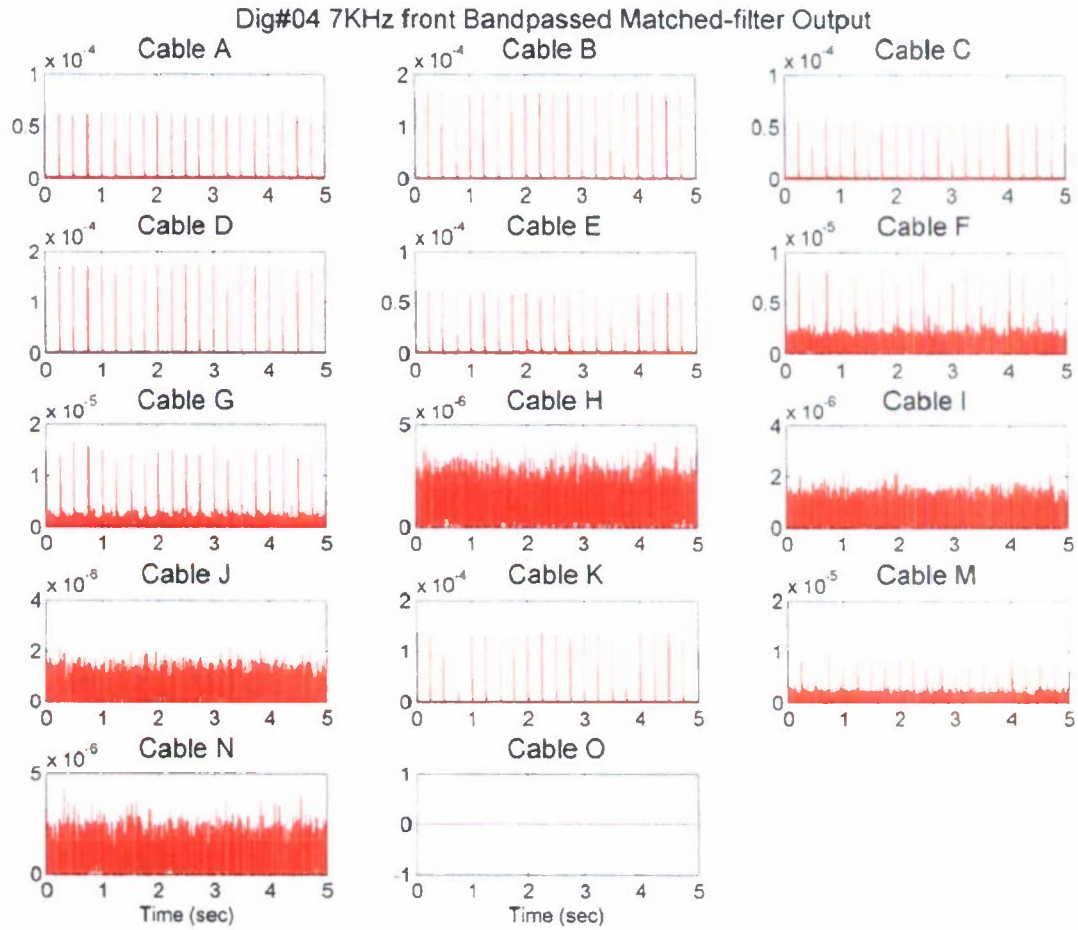


Fig. 21. Overview of acoustic data in Fig. 18, with the spherical transducer in front of the specimen and transmit signal centered at 7 kHz, but following band-pass and matched-filter processing.

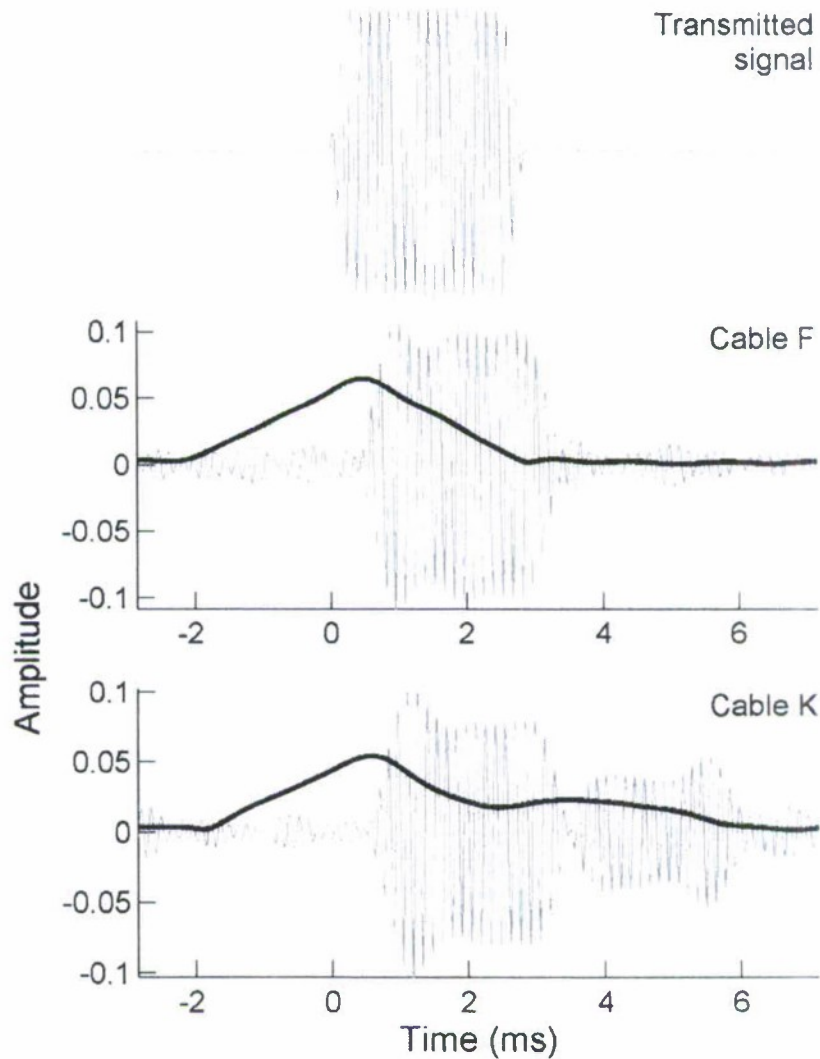


Fig. 22. Detail of processed signals derived from Fig. 17, with the spherical transducer on the right side of the specimen and the transmit frequency centered at 7 kHz. The electronic transmit signal, shown in the upper frame, was recorded on the channel marked Cable Z. Corresponding signals received in the epaxial muscle, Cable F, and melon, Cable K, are shown with their 7-kHz center frequency in the middle and lower frames, respectively. The simple functions shown in the middle and lower frames are the respective matched-filter outputs, derived according to the method in Task 4.

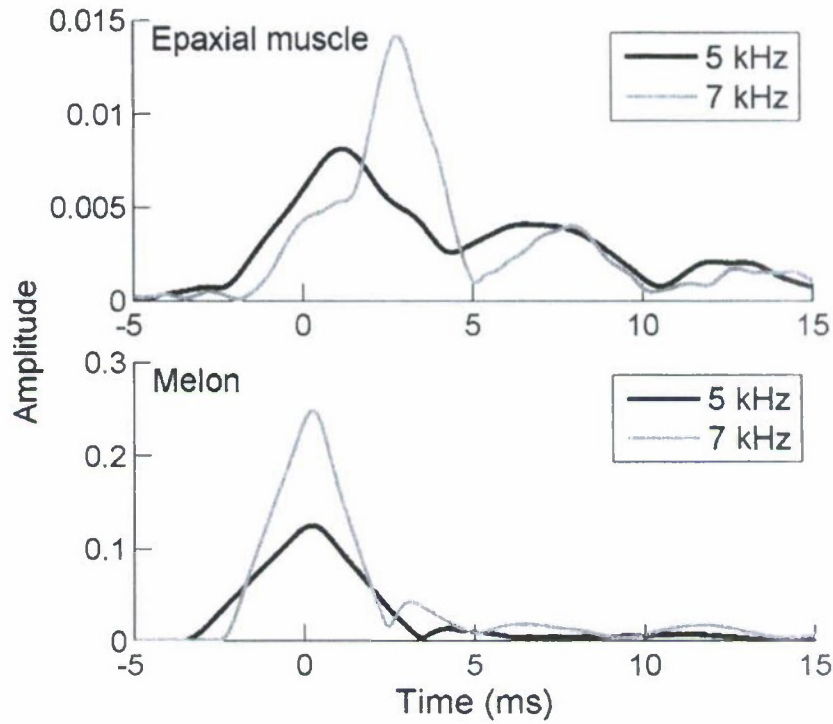


Fig. 23. Matched-filter outputs of 5- and 7-kHz signals received in the epaxial muscle and melon when the acoustic source was positioned in front of the specimen. Each displayed matched-filter output is the average of the 20 corresponding outputs.

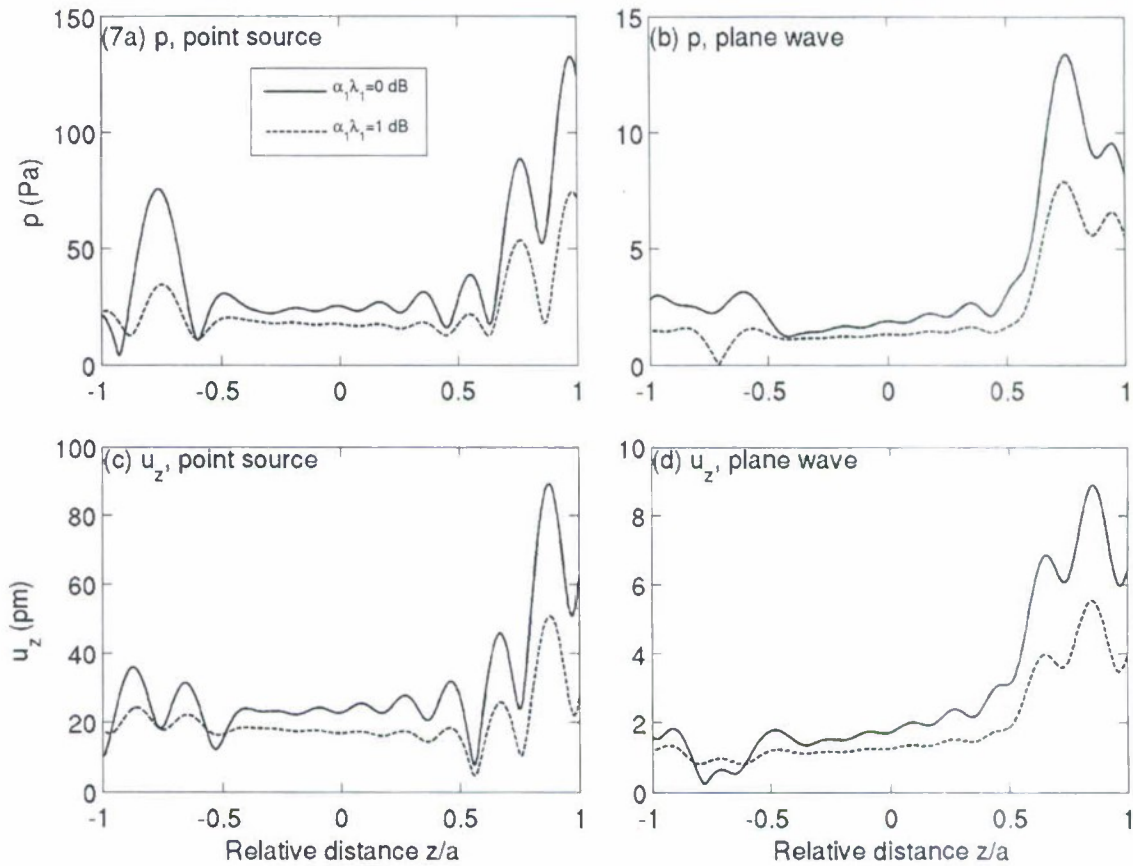


Fig. 24. Pressure and longitudinal particle displacement amplitudes modeled along the longitudinal axis of an immersed 50-mm-diameter fluid sphere at 100 kHz due to ensonification by a spherical wave emanating from a point source of strength 1 Pa m at $z = -75$ mm on the same axis (a,c), and a plane wave of amplitude 1 Pa propagating in the positive z -direction (b,d). The mass density of the fluid sphere is 1900 kg/m^3 , sound speed, 857 m/s, and absorption coefficient, α_1 , 0 or 1 dB per internal wavelength. The mass density of the immersion medium is 1000 kg/m^3 , sound speed, 1500 m/s, and absorption coefficient, 0 dB/m.

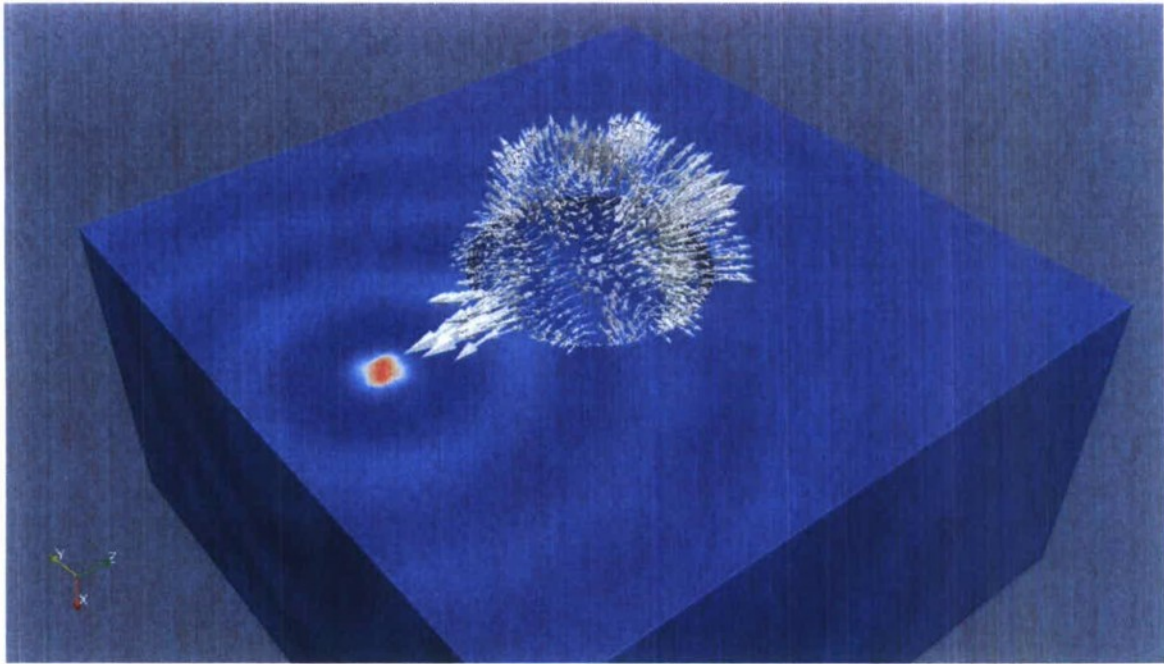


Fig. 25. Pressure field in water (colors) and velocity field (sub-sampled and displayed using arrows) modeled in a spherical shell due to a monopole source. The thin spherical shell was not rendered to permit visualization of the velocity field. Credit: G. Feijoo.

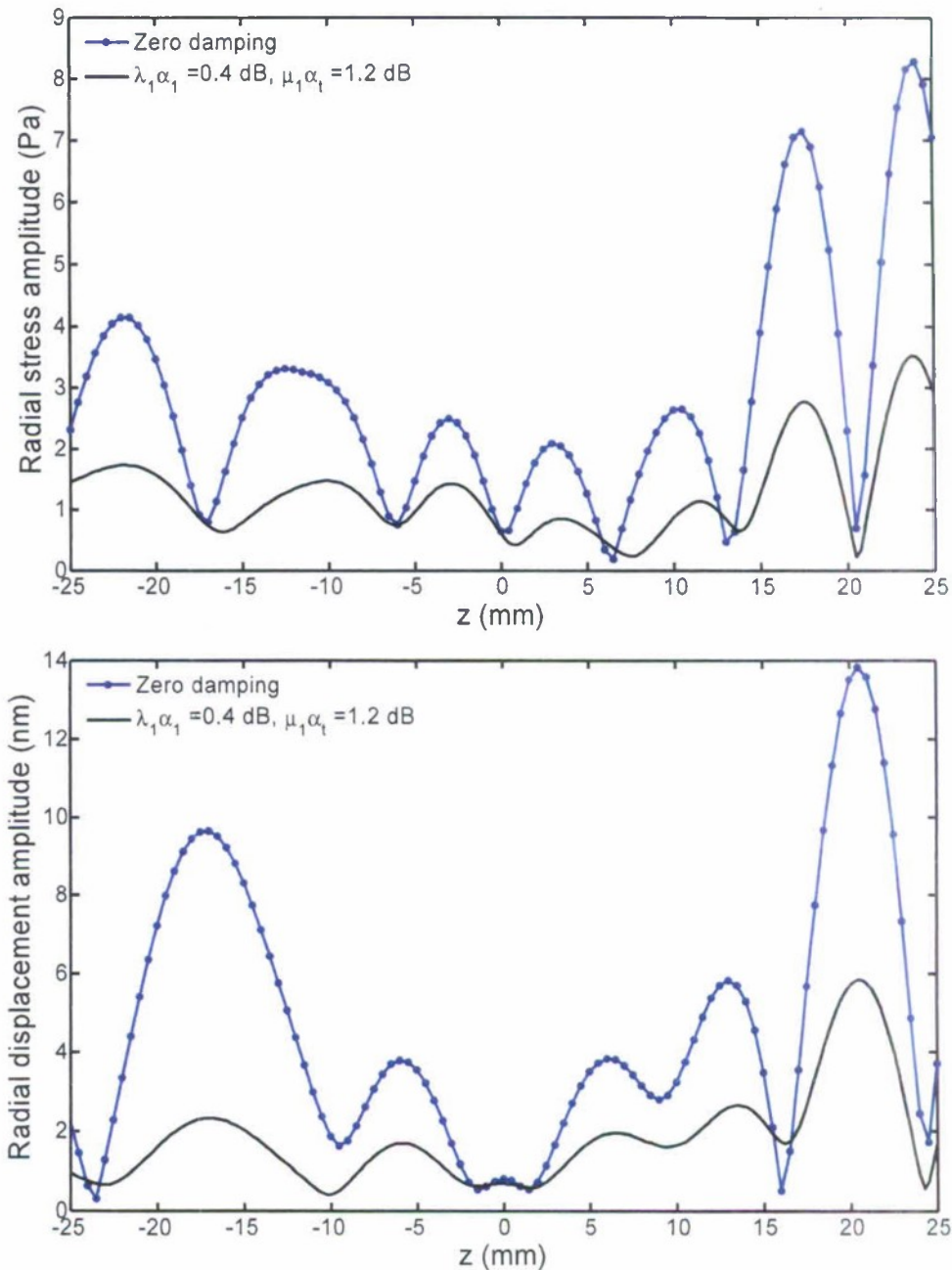
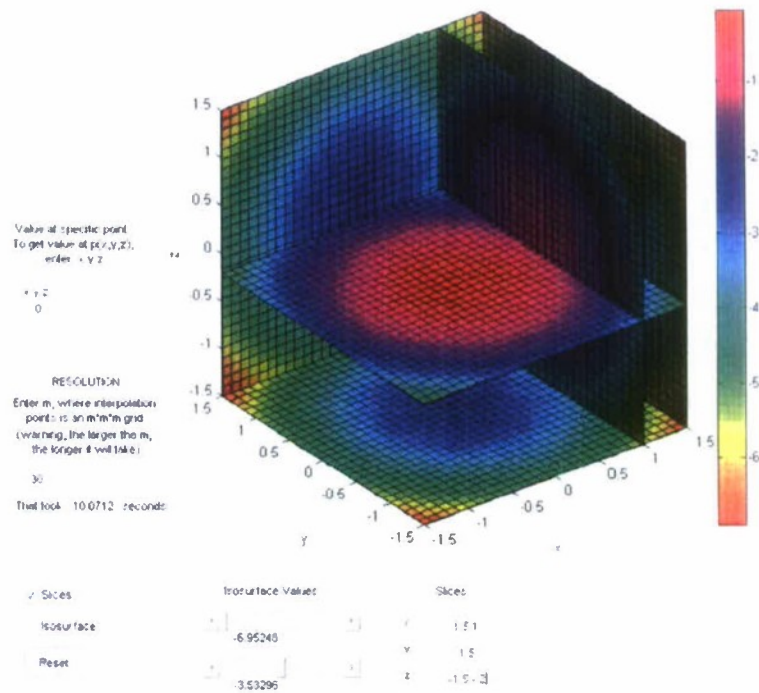
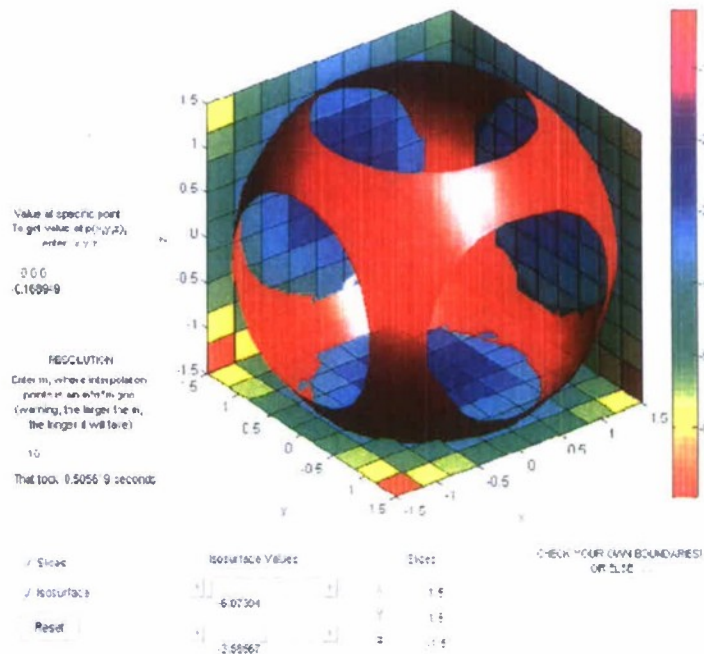


Fig. 26. Radial stress (top) and displacement (bottom) amplitudes modeled inside a 50-mm-diameter sphere of high-density polyethylene due to an incident 100-kHz plane wave of amplitude 1 Pa. The mass density and longitudinal- and transverse-wave sound speeds of the HDPE are 957 kg/m^3 , 2430 m/s , and 950 m/s , respectively. The immersion medium is water, with mass density 1000 kg/m^3 and sound speed 1500 m/s . The computations have been repeated assuming no losses in the sphere and assuming the following values for the product of absorption coefficient and wavelength: 0.40 and 1.20 dB for the respective longitudinal- and transverse-wave sound speed. Credit: D. T. I. Francis.



(a)



(b)

Fig. 27. Virtual Beaked Whale: development of a graphical user interface, with field values of the function $f(x,y,z)=-x^2-y^2-z^2$ shown on the computational boundaries in three orthogonal planes and on (a) two internal, orthogonal slices, and (b) an iso-surface.

Credit: G. Feijoo, L. Cohen.

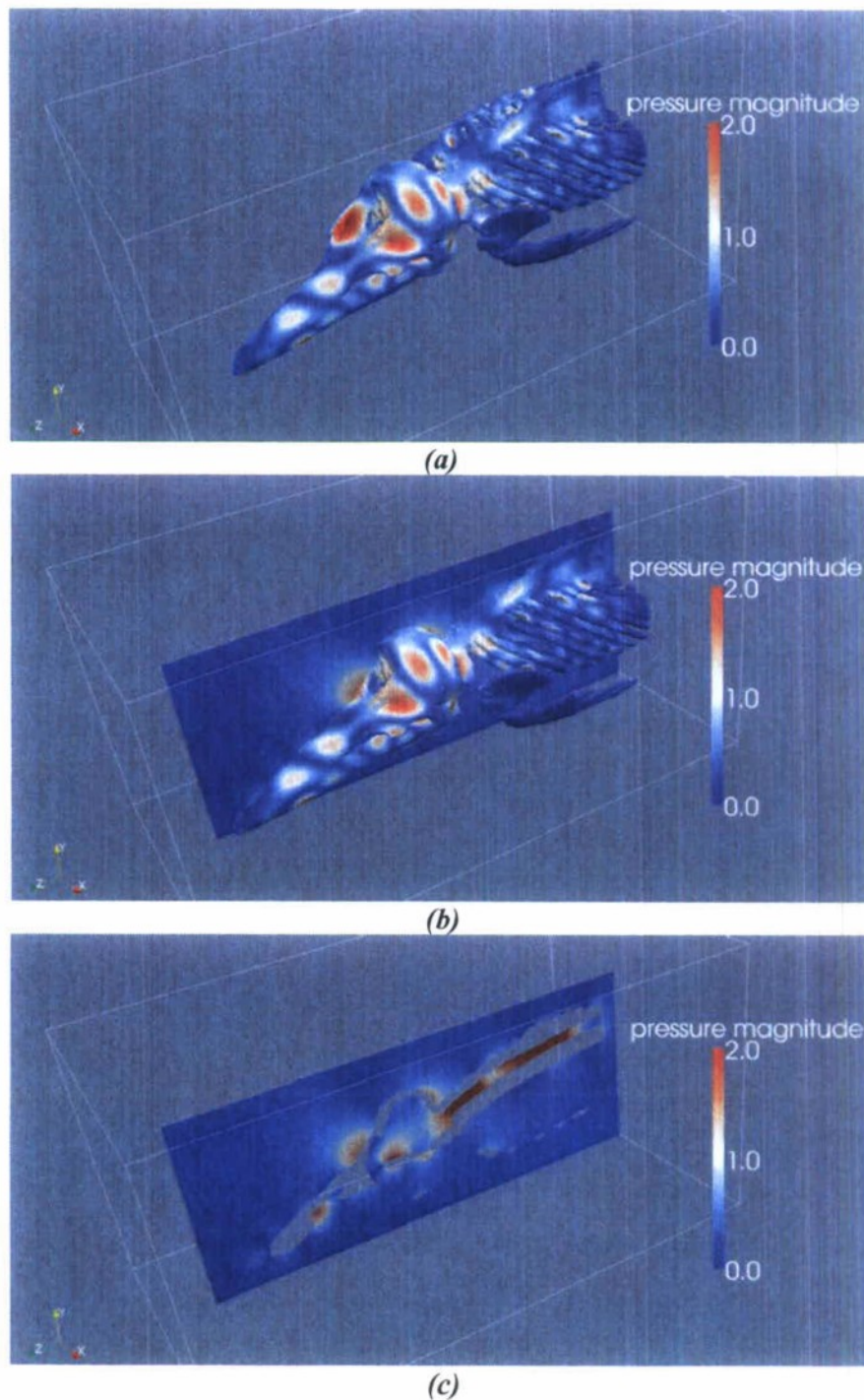


Fig. 28. Virtual Beaked Whale: initial simulations using D_del42 specimen scanned in 2006. The lungs were not modeled, but assumed to have the same properties as the surrounding water. The incident sonar signal is a 5-kHz plane wave moving in the negative z-direction. The magnitude of pressure is simulated on (a) the skeleton, (b) the skeleton and in a sagittal cut, and (c) the sagittal cut only. Credit: G. Feijoo.